



Norwegian University of
Science and Technology

Optimization of passive heave compensation during Subsea Factory heavy lift operations

Weitian Zhou

Marine Technology

Submission date: June 2017

Supervisor: Svein Sævik, IMT

Co-supervisor: Peter Sandvik, Marintek

Norwegian University of Science and Technology
Department of Marine Technology



NTNU – Trondheim
Norwegian University of
Science and Technology

Optimization of Passive Heave Compensation during Subsea Factory Heavy Lift Operation

Weitian Zhou

June 2017

Master Thesis

Department of Marine Technology

Norwegian University of Science and Technology

Supervisor 1: Prof. Svein Sævik, NTNU

Supervisor 2: Peter Sandvik, Marintek

Preface

This master thesis has been finished in June of 2017, which is a further study of the compulsory 7.5 credit project for the 5th year students enrolled in the Marine Technology Master program at NTNU.

The main objective in this thesis is to demonstrate the positive effects of passive heave compensation during subsea heavy lift operation in different environment conditions and find the optimized stroke for the passive heave compensator.

Analysis models provided by Peter Sandvik, Marintek, have been modified in some respects to obtain all the results in this thesis. Guidance given by supervisor Svein Sævik and Peter Sandvik has been very useful regarding introduction to the computer program SIMA and general counselling. In addition, Dr. Yuna Zhao also provided helpful instruction during the process of this thesis.

Trondheim, 2017-06-10

Weitian Zhou

Acknowledgment

I would like to thank the following persons for their great help for my thesis work.

First of all, I am grateful to Professor Svein Sævik, Peter Sandvik and Yuna Zhao, who provide me guidance throughout the whole year. I appreciate the chance to talk with you guys about study, work and also life every week. It motivates me to be positive and hardworking through the whole year and even in my future.

Then, my gratitude goes to Kun Xu, Qidi Wang and Qi Wang, my intelligent friends, who spare no efforts to help me when I was in trouble of software and encourage me a lot when I was in depression. This thesis cannot be finished in time without you guys.

Moreover, I am also grateful to everyone in my office: Lars Gjengseth, Lennard Bösch, Andreas Trollvik, Guttorm Udjus, Suyu Wang and Jialing Yu. It is very great to work with you guys in the last year.

Finally, last but not the least important, I really appreciate what my parents have done for me. I cannot have the chance to study in NTNU and finish my master thesis today without your support.

Thanks for all your encouragement!

Weitian Zhou

NTNU

June 10th, 2017

Abstract

This thesis is about the study of the effect of heave passive compensation during subsea factory heavy lift operations. All the analysis are based on the data provided by Peter Sandvik, Marintek. The main objective is to demonstrate the positive effect of passive heave compensation and determine the optimized stroke of passive heave compensator by the static and dynamic analysis in SIMA program.

The literature study is based on articles related to heave compensation during marine operation and DNV-RP-H103, which provides guidance for modelling and analysis of marine operations. The different types of heave compensator with different applications are introduced in the thesis.

Then, an introduction of SIMA program will be presented in chapter 4. Meanwhile how the models of environment conditions, different bodies and coupling specifications, as well as the calculation parameters are established in SIMA is illustrated in chapter 5.

Moreover, five cases are performed in this thesis to prove that the passive heave compensator will contribute to the reduction of dynamic loads and motions during heavy lift operation. The analysis is performed in SIMA, a workbench used to solve tasks during marine operations. The lifting module is modelled as a combination of four same mudmat and the passive heave compensator is modelled by a fixed elongation coupling between the hook and cranemaster. As for the model without passive heave compensator, it just replaces the fixed elongation coupling between the hook and cranemaster with a simple coupling wire. And all the results from SIMA will be plotted in chapter 6.

In the last chapter, the conclusion is drawn. It proves that the passive heave compensator has an effect of alleviating vertical forces and motions during heavy lift operation. Meanwhile it also demonstrates that the optimized PHC has the same influence as the initial PHC (passive heave compensator). At last, the recommendation for further work is given.

Contents

Preface	i
Acknowledgment	ii
Abstract	iii
1 Introduction	2
1.1 Background	2
1.2 Objectives	3
1.3 Limitations	4
1.4 Structure of the thesis	4
2 Literature study	5
2.1 Heavy lift operation	5
2.2 Heave compensator	6
2.3 Passive heave compensator	7
2.3.1 Definition	7
2.3.2 Working principle	8
2.3.3 Effects and efficiency	8
2.3.4 Limitation	9
2.4 Active heave compensator	10
2.5 Combined heave compensator	11
3 DNV-RP-H103	13
3.1 General	13
3.2 Landing on seabed	13

3.2.1	Introduction	13
3.2.2	Physical parameters and effects	14
3.2.3	Calculation of skirt penetration resistance	15
4	Introduction of SIMA	16
4.1	Theoretical basis of SIMA	16
4.2	SIMA characteristics	17
4.2.1	Coordinate system	17
4.2.2	Unit and physical constraints	18
4.2.3	Coupling specifications	19
5	Modelling components in SIMA	21
5.1	Introduction of the model in SIMA	21
5.2	Location modelling	22
5.3	Environment modelling	23
5.4	Bodies modelling	24
5.4.1	Ship modelling	24
5.4.2	Cranemaster modelling	25
5.4.3	Hook modelling	25
5.4.4	Manifold and protection structure modelling	26
5.4.5	Mudmat modelling	27
5.5	Coupling modelling	29
5.5.1	Simple wire couplings	30
5.5.2	Fixed elongation coupling	31
5.6	Calculation parameters modelling	34
5.6.1	Static calculation modelling	35
5.6.2	Dynamic calculation modelling	35
6	Results and analysis	38
6.1	Static Analysis	38
6.2	Dynamic Analysis	39
6.2.1	Dynamic analysis on Mudmat	40

6.2.2	Dynamic analysis on Crane wire	44
6.2.3	Dynamic analysis of optimized PHC	50
6.3	Discussion	56
7	Conclusion	60
7.1	Conclusion	60
7.2	Recommendations for further work	61
A	Vertical coupling system force in mudmats	62
B	Vertical global velocity of mudmats	67
	Bibliography	72

List of Figures

Fig. 1.1	SIMOPS - Simultaneous Operations system designed by Kongsberg	2
Fig. 2.1	Heavy Lift Operations in Asia Pacific	6
Fig. 2.2	An approximate timeline of heave compensation development(1)	6
Fig. 2.3	Passive heave compensator	8
Fig. 2.4	Efficiency of typical passive heave compensator(2)	9
Fig. 2.5	Active heave compensator(3)	10
Fig. 2.6	Combined heave compensator	11
Fig. 3.1	Model for impact analysis(4)	14
Fig. 4.1	Local strip coordinate system,XS	17
Fig. 4.2	Coordinate system[XS,YS,ZS] of the slender element(5)	18
Fig. 5.1	Part of the model in SIMA	21
Fig. 5.2	Location modelling in SIMA	22
Fig. 5.3	Environment modelling of case1 in SIMA	23
Fig. 5.4	Ship modelling in SIMA	24
Fig. 5.5	Ship body setting in SIMA	24
Fig. 5.6	Cranemaster modelling in SIMA	25
Fig. 5.7	Cranemaster body setting in SIMA	25
Fig. 5.8	Hook modelling in SIMA	25
Fig. 5.9	Hook body setting in SIMA	25
Fig. 5.10	ISS modelling in SIMA	26

Fig. 5.11	ISS body setting in SIMA	26
Fig. 5.12	ISS Slender element 1 in SIMA	27
Fig. 5.13	Mudmat FS modelling in SIMA	28
Fig. 5.14	Mudmat FS body setting in SIMA	28
Fig. 5.15	Hydrodynamic data on Mudmat FS in SIMA	28
Fig. 5.16	Soil penetration on Mudmat FS in SIMA	29
Fig. 5.17	Sling FS modelling in SIMA	30
Fig. 5.18	Lifting wire modelling in SIMA	31
Fig. 5.19	Restriction modelling of mudmat FS in X-direction in SIMA	32
Fig. 5.20	Crane wire modelling in SIMA	32
Fig. 5.21	Force interpolation of crane wire in SIMA	33
Fig. 5.22	Force interpolation of crane wire in SIMA	33
Fig. 5.23	Crane wire measurement modelling in SIMA	34
Fig. 5.24	Static calculation modelling in SIMA	35
Fig. 5.25	General dynamic calculation modelling in SIMA	36
Fig. 5.26	Storage information of the dynamic calculation in SIMA	36
Fig. 6.1	Vertical coupling force in Mudmat FS with PHC, Case1	40
Fig. 6.2	Vertical coupling force in Mudmat FS without PHC, Case1	40
Fig. 6.3	Vertical velocity of Mudmat FS with PHC, Case1	40
Fig. 6.4	Vertical velocity of Mudmat FS without PHC, Case1	40
Fig. 6.5	Vertical global translation of Mudmat FS with PHC, Case1	40
Fig. 6.6	Vertical global translation of Mudmat FS without PHC, Case1	40
Fig. 6.7	Vertical coupling force in Mudmat FS with PHC, Case2	42
Fig. 6.8	Vertical coupling force in Mudmat FS without PHC, Case2	42
Fig. 6.9	Vertical velocity of Mudmat FS with PHC, Case2	42
Fig. 6.10	Vertical velocity of Mudmat FS without PHC, Case2	42
Fig. 6.11	Vertical coupling force in Mudmat FS with PHC, Case3	42
Fig. 6.12	Vertical coupling force in Mudmat FS without PHC, Case3	42
Fig. 6.13	Vertical velocity of Mudmat FS with PHC, Case3	42

Fig. 6.14	Vertical velocity of Mudmat FS without PHC, Case3	42
Fig. 6.15	Vertical coupling force in Mudmat FS with PHC, Case4	43
Fig. 6.16	Vertical coupling force in Mudmat FS without PHC, Case4	43
Fig. 6.17	Vertical velocity of Mudmat FS with PHC, Case4	43
Fig. 6.18	Vertical velocity of Mudmat FS without PHC, Case4	43
Fig. 6.19	Vertical coupling force in Mudmat FS with PHC, Case5	43
Fig. 6.20	Vertical coupling force in Mudmat FS without PHC, Case5	43
Fig. 6.21	Vertical velocity of Mudmat FS with PHC, Case5	43
Fig. 6.22	Vertical velocity of Mudmat FS without PHC, Case5	43
Fig. 6.23	Coupling system force in crane wire, Case1	44
Fig. 6.24	Coupling system force in crane wire measurement, Case1	45
Fig. 6.25	Coupling system force in crane wire, Case2	46
Fig. 6.26	Coupling system force in crane wire measurement, Case2	46
Fig. 6.27	Coupling system force in crane wire, Case3	47
Fig. 6.28	Coupling system force in crane wire measurement, Case3	47
Fig. 6.29	Coupling system force in crane wire, Case4	48
Fig. 6.30	Coupling system force in crane wire measurement, Case4	48
Fig. 6.31	Coupling system force in crane wire, Case5	49
Fig. 6.32	Coupling system force in crane wire measurement, Case5	49
Fig. 6.33	Crane wire modelling with optimized stroke in SIMA	50
Fig. 6.34	Vertical coupling force in Mudmat FS with optimized PHC, Case1	51
Fig. 6.35	Vertical velocity of Mudmat FS with optimized PHC, Case1	51
Fig. 6.36	Vertical coupling force in Mudmat FS with optimized PHC, Case2	52
Fig. 6.37	Vertical velocity of Mudmat FS with optimized PHC, Case2	52
Fig. 6.38	Vertical coupling force in Mudmat FS with optimized PHC, Case3	53
Fig. 6.39	Vertical velocity of Mudmat FS with optimized PHC, Case3	53
Fig. 6.40	Vertical coupling force in Mudmat FS with optimized PHC, Case4	54
Fig. 6.41	Vertical velocity of Mudmat FS with optimized PHC, Case4	54
Fig. 6.42	Vertical coupling force in Mudmat FS with optimized PHC, Case5	55
Fig. 6.43	Vertical velocity of Mudmat FS with optimized PHC, Case5	55

Fig. A.1	Vertical coupling system force in Mudmat FP, Case 1	62
Fig. A.2	Vertical coupling system force in Mudmat AS, Case 1	62
Fig. A.3	Vertical coupling system force in Mudmat AP, Case 1	63
Fig. A.4	Vertical coupling system force in Mudmat FP, Case 2	63
Fig. A.5	Vertical coupling system force in Mudmat AS, Case 2	63
Fig. A.6	Vertical coupling system force in Mudmat AP, Case 2	63
Fig. A.7	Vertical coupling system force in Mudmat FP, Case 3	64
Fig. A.8	Vertical coupling system force in Mudmat AS, Case 3	64
Fig. A.9	Vertical coupling system force in Mudmat AP, Case 3	64
Fig. A.10	Vertical coupling system force in Mudmat FP, Case 4	64
Fig. A.11	Vertical coupling system force in Mudmat AS, Case 4	65
Fig. A.12	Vertical coupling system force in Mudmat AP, Case 4	65
Fig. A.13	Vertical coupling system force in Mudmat FP, Case 5	65
Fig. A.14	Vertical coupling system force in Mudmat AS, Case 5	65
Fig. A.15	Vertical coupling system force in Mudmat AP, Case 5	66
Fig. B.1	Vertical global velocity of Mudmat FP, Case 1	67
Fig. B.2	Vertical global velocity of Mudmat AS, Case 1	67
Fig. B.3	Vertical global velocity of Mudmat AP, Case 1	68
Fig. B.4	Vertical global velocity of Mudmat FP, Case 2	68
Fig. B.5	Vertical global velocity of Mudmat AS, Case 2	68
Fig. B.6	Vertical global velocity of Mudmat AP, Case 2	68
Fig. B.7	Vertical global velocity of Mudmat FP, Case 3	69
Fig. B.8	Vertical global velocity of Mudmat AS, Case 3	69
Fig. B.9	Vertical global velocity of Mudmat AP, Case 3	69
Fig. B.10	Vertical global velocity of Mudmat FP, Case 4	69
Fig. B.11	Vertical global velocity of Mudmat AS, Case 4	70
Fig. B.12	Vertical global velocity of Mudmat AP, Case 4	70
Fig. B.13	Vertical global velocity of Mudmat FP, Case 5	70
Fig. B.14	Vertical global velocity of Mudmat AS, Case 5	70

Fig. B.15 Vertical global velocity force of Mudmat AP, Case 5 71

List of Tables

Tab. 3.1	Correlation coefficients for skin friction and tip resistance in sand and over-consolidated clay	15
Tab. 4.1	Input data units set	19
Tab. 5.1	The body weights of the model in SIMA	22
Tab. 5.2	Physical constants in location modelling	22
Tab. 5.3	Environment conditions	23
Tab. 5.4	End points and types of the wires	30
Tab. 6.1	Static body positions of underwater structures	38
Tab. 6.2	Vertical positions deviation	38
Tab. 6.3	Coupling forces and moments in wires	39
Tab. 6.4	Related information about dynamic analysis	39
Tab. 6.5	Optimized results of Mudmat FS in case 1	41
Tab. 6.6	Coupling system force in Crane wire measurement	45
Tab. 6.7	Vertical coupling system force in Mudmat FS	56
Tab. 6.8	Vertical global velocity of Mudmat FS	57
Tab. 6.9	Vertical coupling system force in Mudmat FS compared between optimized and initial PHC	58
Tab. 6.10	Vertical global velocity of Mudmat FS compared between optimized and initial PHC	59

Chapter 1

Introduction

1.1 Background

Marine operation is of great importance in offshore industry where the needs for advanced technology in deep water always exists. Figure 1.1 shows a simultaneous operation system designed by Kongsberg.



Figure 1.1: SIMOPS - Simultaneous Operations system designed by Kongsberg

With the increasing demand for energy, most of whose resources are non-renewable like oil and

gas, large developments are made in marine operation. The latest research are mainly based on large new gas field with more complex subsea operation while the early fields focused on shallow waters operation. Typical marine operations include:

- Seismic survey
- Pipe lay
- Module installation
- Inspection, maintenance and repair(6)

Nowadays, most of the marine operations are achieved by advanced equipped specialized vessels for the challenging tasks.

One of the important marine operations is subsea factory heavy lift operation, which consists of various operational phases: lifting in the air, lowering through the splash zone, lowering down to seabed and seabed landing(7). During the process of subsea factory heavy lift operation, the main challenge is how to reduce the amplified vertical motions and forces caused.

The purpose of this project is to investigate measures of reducing the transient motions during the subsea module installation. Sever damages might occur in the phase of seabed landing, thus passive heave compensators (PHC) are applied during heavy lift operations. The task is to identify the influence of PHC during different weather environments and the optimum stroke of PHC. The results will help to optimize the PHC and enhance the efficiency.

1.2 Objectives

The main objectives of this Master's thesis are:

1. Literature study, including relevant standards for lift operations and different types of heave compensators, theoretical basis for computational tools like SIMA.
2. Establish models as case studies to evaluate the lift operation responses. All the input data are provided by co-advisor Peter Sandvik, Marintek.

3. Perform analysis in SIMA to demonstrate that the models established in objective 2 are working.
4. Investigate and determine the optimum heave compensator stroke.
5. Focus on that whether the heave compensator is capable of evening out the dynamic response when the object penetrates in to the seabed.

1.3 Limitations

In the present study, the passive heave compensator is just modelled by a fixed elongation coupling and the analysis is based on time domain. In order to get a more accurate result, the time step should be sufficiently small. Besides that, the environment conditions are only defined by wave in this thesis.

1.4 Structure of the thesis

The rest of the thesis is structured as follows. In Chapter 2, it gives an introduction to heavy lift operation and heave compensators. The literature study of DNV-RP-H103 is discussed in Chapter 3. Further, Theory and methodology of SIMA will be presented in Chapter 4. In Chapter 5, it illustrates the method of modelling components in SIMA. And In chapter 6 and 7, environment data setting and dynamic analysis are presented. The conclusion and suggestions for the further study in the master thesis will be discussed in Chapter 7.

Chapter 2

Literature study

2.1 Heavy lift operation

The development of early offshore fields which were established in shallow waters is limited by the capacity of offshore cranes. Even for small modules, the operation work was still time consuming and costly. As the enhancement of lifting capacity of cranes, the way of how offshore fields develop is modified, which reduces the working time and cost effectively.

Due to most of the discovered large gas and oil fields in shallow waters have already been developed, new technology should be performed to exploit smaller and more complex fields.

Nowadays, the offshore fields development are mainly based on the subsea technology, which is reliable and cost efficient(6).

Lifting forms part of almost every offshore and subsea operation, ranging from lifting of stores and spares to complicated and heavy lifts. Over 200 different lifting operations can take place on a single vessel, each with the possibility of injury to people and damage to equipment, but with proper planning, hazards can be identified and risks can be reduced or eliminated.

A typical subsea factory heavy lift operation consists of 4 main operational phases:deck lift off, wave zone lower through, deepwater lower down and seabed entrance.

Amplified vertical motions and forces of equipment can be caused by axial resonance of wire during different phases of heavy lift operation. The challenge is to reduce the vertical oscillatory motion of the modules and forces when the modules enter into seabed. Figure 2.1 shows an example on heavy lift operation in Asia Pacific.



Figure 2.1: Heavy Lift Operations in Asia Pacific

2.2 Heave compensator

All marine operations are dependent on environment conditions, which should be monitored and recorded to perform them safely. Additionally, a specific detailed operation plan and advanced equipment are of great significance as well.

Equipment handling can be a difficult task, especially for bad sea states. During heavy lift operation, heave compensator system can be used to alleviate to reduce the vertical motions and forces. The past 40 years have witnessed heave compensator systems to become common used in many marine operations. Figure 2.2 shows the major developments of heave compensators during the past 40 years.

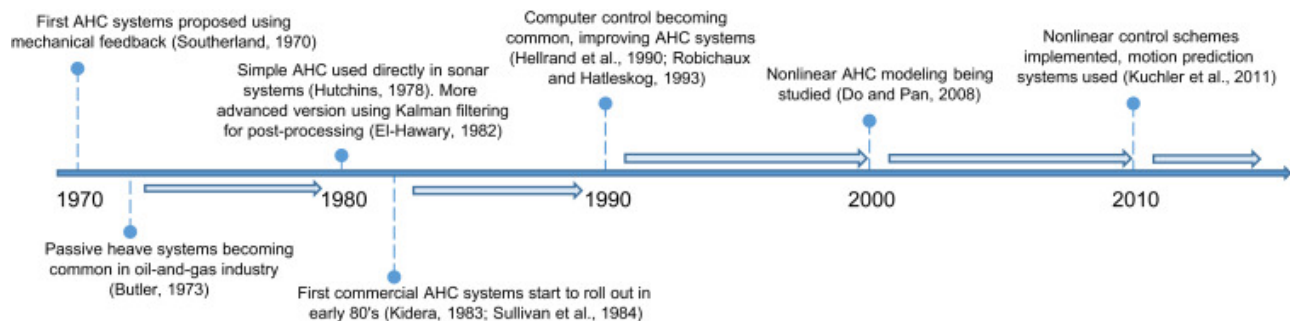


Figure 2.2: An approximate timeline of heave compensation development(1)

Heave compensator was suggested to be used in marine operations by Southerland in 1970. And after the success of Butler's test of passive heave compensators, it became widely accepted and commonly used in oil and gas industry. With the development of computational technology, heave compensators were modified with better system modelling as well as more accurate

control, which makes both passive and active heave compensators widespread in oil and gas industry.

There are three types of heave compensators typically used in marine operations, which are passive heave compensator (PHC), active heave compensator (AHC) and combined heave compensator. The passive system is designed to maintain a constant line tension, while a simple mechanical feedback system is applied in the active system to adjust for the ship heave motions. The detail information about them will be introduced in the following sections.

2.3 Passive heave compensator

2.3.1 Definition

Passive heave compensator is defined as "an offshore equipment, generally connected between the crane hook and the payload, such that it stores the energy from waves influencing the payload and dissipate it later" (2).

It means little or no external support is needed for the passive compensation system. It consists of few and simple components which are easy to maintain (8), and thus it has an advantage of simplicity and cheaper budget. Generally, a passive heave compensator is based on a spring-damper system which includes cylinder, piston, nozzles and accumulator. An example a passive heave compensator system with a double acting hydraulic load absorber is presented in Figure 2.3.

The cylinder contains hydraulic fluid inside while Nitrogen fills the gas accumulator. The range of the pressure change in the compensator depends on the volume of the gas in the accumulator. There is a limit of stroke in this unit, which can not be exceeded. It will lead to failure of the passive heave compensator if the limit is exceeded during the heavy lift operations.

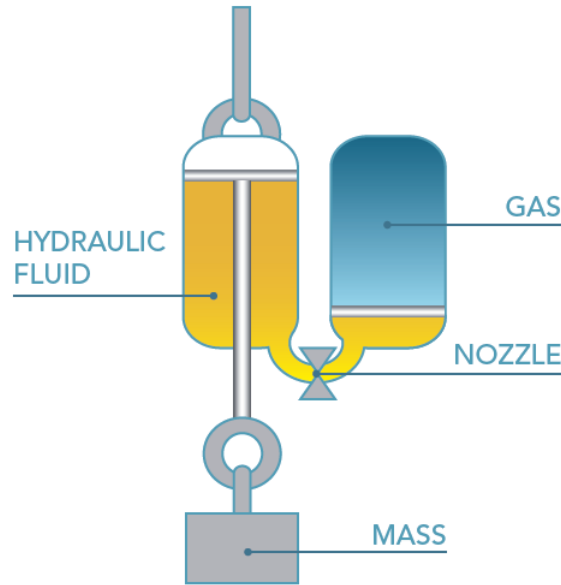


Figure 2.3: Passive heave compensator

2.3.2 Working principle

The passive heave compensator doesn't need any input of energy during operation(4). In figure 2.3, payload is given by the mass which is attached to the lower end of the compensator, which leads the motion of the piston rod. When the piston rod moves downwards, the hydraulic fluid in the cylinder is forced to enter the accumulator through nozzle between them. The nozzle can be used as damper to limit the fluid velocity. Meanwhile, the gas in the accumulator is compressed by the motion of fluid, acting like spring.

As a result of that, the combination of the damping and spring effect contributes to the reduction of forces and motions during heavy lift operations.

The stiffness of the passive heave compensator is linearised with the pressure of the accumulator, which depends on the motion of the piston. And the damping is dependent on the stroke velocity.

2.3.3 Effects and efficiency

During the heavy lift operation, passive heave compensator is used to alleviate the dynamic loads and motions. The transfer function is defined as the ratio of the amplitude of response

and amplitude of excitation.

$$H(w) = \frac{\eta_3}{\eta_{3T}} \quad (2.1)$$

In equation 2.1, $H(w)$ is the complex transfer function, and η_3 is the amplitude of response heave motion while η_{3T} is the amplitude of the excitation motion. Based on the transfer function $H(w)$ given above, the efficiency of the passive heave compensator can be calculated by:

$$e = 1 - |H(w)| \quad (2.2)$$

In equation 2.2, e stands for the efficiency of the passive heave compensator, from which whether the compensator makes positive contribution to the heavy lift operation can be found.

When the natural frequency is ω_0 , damping as well as the stiffness of the passive heave compensator is relatively small, the drag force and added mass are very large meanwhile, the efficiency of heave is given with the wave period and payload mass density in Figure 2.4(9).

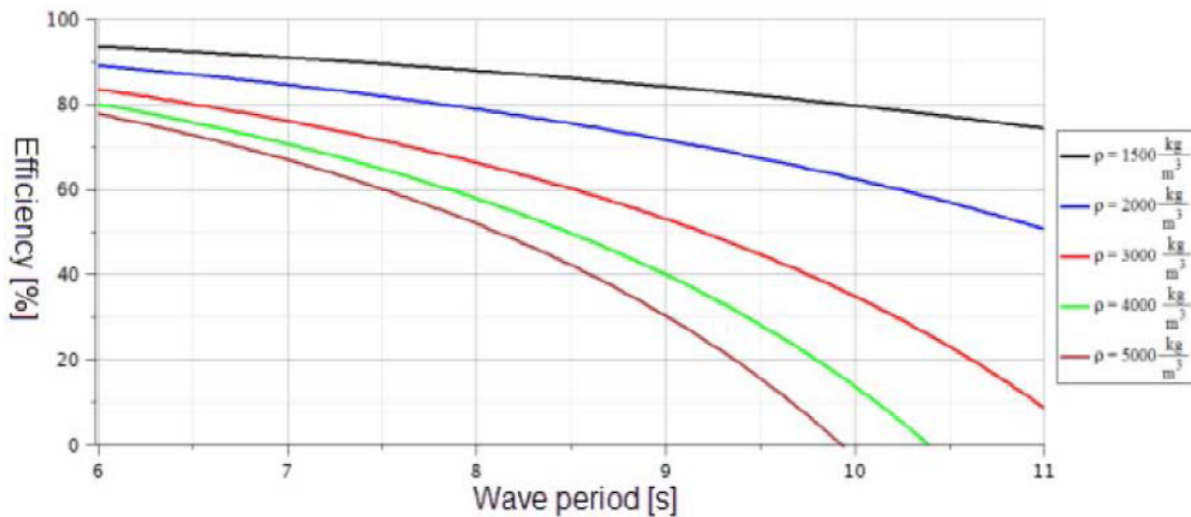


Figure 2.4: Efficiency of typical passive heave compensator(2)

2.3.4 Limitation

The limited volume of cylinder and accumulator restricts the gas volume and the range of pressure change. Additionally, it is not possible to modify the gas pressure when the operation is

processing with passive heave compensators. For those with large gas volume, obviously, it will show better compensation ability. However it will take more time to vary the gas pressure at the same time. Due to there is no energy consumption during the operation, pre-charged accumulators are required before the operation.

2.4 Active heave compensator

Active heave compensation system is based on the signal detection and analysis to measure the heave motion of ship and then provide a proper heave compensation. It has high versatility and more accuracy as well as flexibility with the change of heave motion.

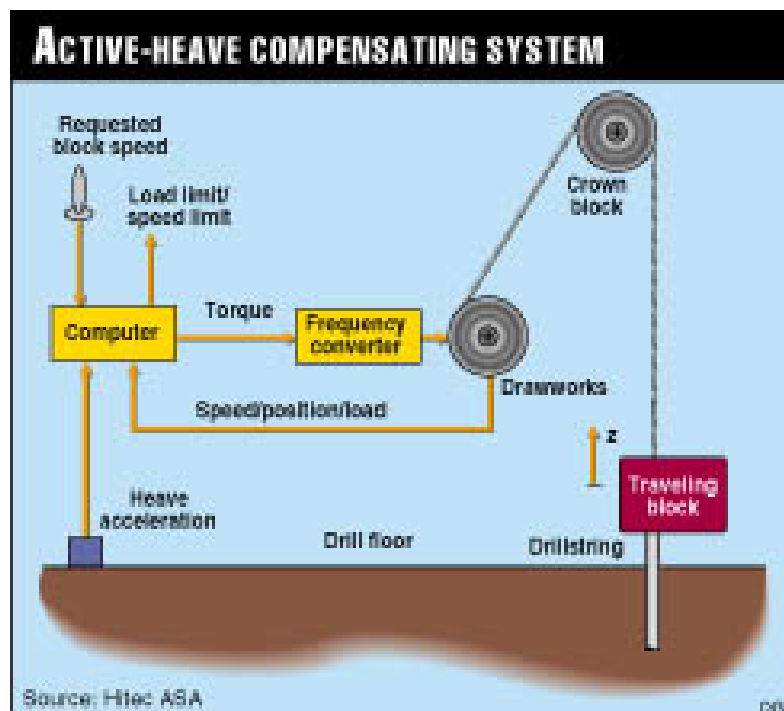


Figure 2.5: Active heave compensator(3)

Compared with passive heave compensation system, there is a closed circuit in active heave compensator and input energy is required. The measure of ship heave motion and the proper reflection of the active compensator are based on support equipment, such as sensors, actuators and computers. These advanced facilities also bring some drawback at the same time. They make the system more complex with higher cost. And the failure of any single equipment needed for this system can lead to inefficiency or dangerous situations.

With a strict active heave compensator, not only can the system face equipment failure, but additional power supply for the whole system must be taken into account. The actuators need to be powered either hydraulically or electrically all the working times to ensure the expected system operation. All these might be the limitation to the application of active heave compensators.

2.5 Combined heave compensator

Combined heave compensators, presented in Figure 2.6, benefit both from advantages of passive and active heave compensators. There are both passive and active cylinder in a combined compensation system. A passive cylinder can be used to carry the load while an active cylinder contributes to friction losses. In addition, it overcomes the limit of the two kinds of heave compensator system. As mentioned above, a passive heave compensator is limited by the gas volume and power supply should be considered in active heave compensator design. If gas volume and power delivery are restriction factor, a combined heave compensator will be an optimal option as it doesn't need the full load to be held totally passively or actively.

The combined compensator designed by Hatleskog and Dunnigan in 2007 uses the passive

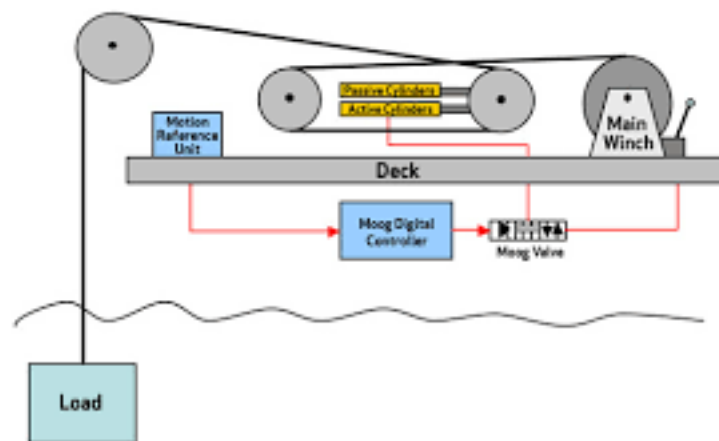


Figure 2.6: Combined heave compensator

system to afford the bulk load while the active system is used to adjust in further load vibration. From their report, only an actuator with capability of 100,000 lbf is needed to afford a 1,000,000 lbf passively held load(10). It is similar to the patent given by Robichaux and Hatleskog

in 1993(11). Compared to active compensation system, combined heave compensator system doesn't need any energy input while the system is simpler. However, the cost of equipment for active heave compensator still needs to be taken into account, which is the limited factor of combined heave compensators.

Chapter 3

DNV-RP-H103

3.1 General

RP is the abbreviation of "Recommended Practice". DNV-RP-H103 is referred as guidance for modelling and analysis of marine operations, especially for different phases of lifting operation(4). It provides simplified formulations for design loads during lifting through wave zone, deepwater lowering operation, landing on seabed and retrieval as well as towing operation. The focus of the present case is on the load during landing on seabed.

3.2 Landing on seabed

3.2.1 Introduction

It is necessary to evaluate the loads when landing on seabed, which can be used to confirm whether foundation failure and damage to sensitive equipment happen during landing.

Only the degree of freedom of vertical motion is considered when simulating the landing of a bucket on the seabed. The model for impact analysis is depicted in Figure 3.1. The geometry of the anchor is simplified as a cylinder with height L and diameter D . A hatch for water evacuation with area A_h is modeled on the top and δ_{soil} stands for the rate of change of soil displacement.

The impact analysis is based on calculation by time integration of the general equation of mo-

tion. In order to solve it by time integration, the instant time dependent values of all relevant forces applied on the anchor should be taken into account.

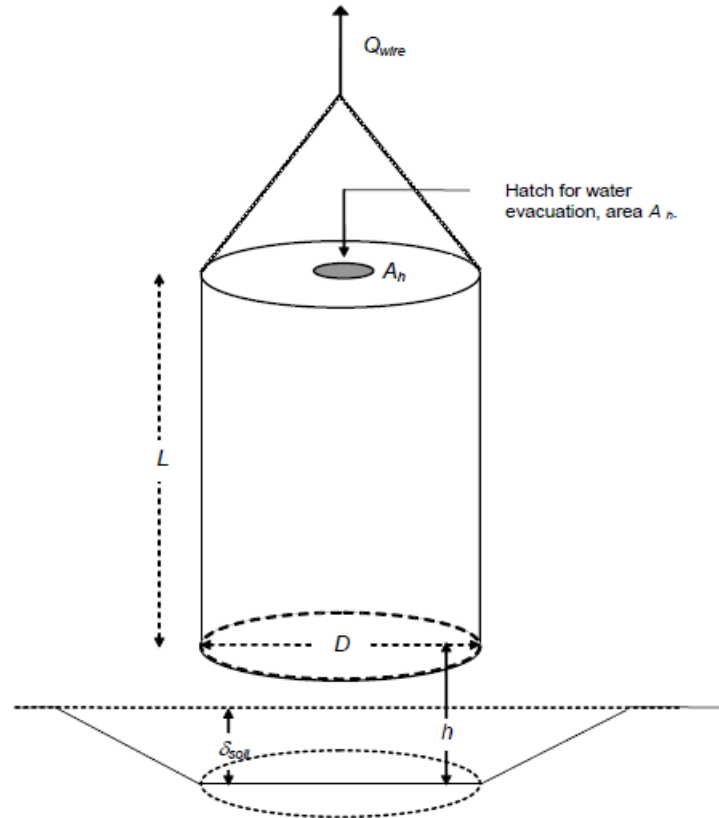


Figure 3.1: Model for impact analysis(4)

3.2.2 Physical parameters and effects

The structural mass for calculation consists of structural elements and equipment on top of the bucket. The added mass for a typical foundation bucket can be calculated by:

$$A_{33} = \rho \cdot A_b \cdot L \cdot \left(1 + \frac{2D}{3L}\right) \quad (3.1)$$

where A_{33} is the added mass for vertical motion [kg], D is the diameter of anchor [m], L is the length of anchor [m], and A_b is the anchor area [m^2] which is equal to $\frac{\pi D^2}{4}$.

Based on equation 3.1, the total dynamic mass M' and the initial kinetic energy can be found by:

$$M' = M + A_{33} \quad (3.2)$$

$$E_{k0} = \frac{1}{2} \cdot M' \cdot v_{c0}^2 \quad (3.3)$$

3.2.3 Calculation of skirt penetration resistance

The skirt penetration resistance is given by equation 3.4, which is the sum of the vertical shear resistance.

$$Q_{skirt} = A_s \cdot \int_0^d f(z) dz + A_t \cdot q_t(d) \quad (3.4)$$

Where Q_{skirt} is the skirt penetration resistance [N], d is the depth of penetration [m], A_s and A_t represent friction area per meter depth [m^2/m] and skirt tip area [m^2] respectively while $f(z)$ and $q_t(d)$ stand for skin friction at depth z [N/m^2] and tip resistance at the depth of penetration [N/m^2] respectively.

The skin friction and tip resistance are given by:

$$f(z) = k_f \cdot q_c(z) \quad (3.5)$$

$$q_t(z) = k_t \cdot q_c(z) \quad (3.6)$$

where $q_c(z)$ is the cone penetration resistance as measured in a cone penetration test [N], and the coefficient of skin friction and tip resistance are given by table 3.1.

Table 3.1: Correlation coefficients for skin friction and tip resistance in sand and over-consolidated clay

Correlation coefficient	Sand		Clay	
	Most probable	Highest expected	Most probable	Highest expected
Skin fiction, k_f	0.03	0.05	0.001	0.003
Tip resistance, k_t	0.4	0.6	0.3	0.6

Chapter 4

Introduction of SIMA

4.1 Theoretical basis of SIMA

SIMA is a workbench developed as a Joint Industry Project by Marintek and Statoil to model and analyze tasks related to marine operation. It supports execution of both individual simulation and execution of several simulations through workflow. The engine workflow makes it possible to analyze multiple variations of an analysis. To simplify a complex file management with many simulations, workbench can take care of all the results and files that are generated by the numerical engine.

The dynamic analysis of SIMA is based on time integration. And the results are calculated from equilibrium equations step by step in time domain. In addition, a post processor is included in SIMA which can be used to process the obtained data.

Typical tasks in SIMA include:

- Underwater installations
- Unloading
- Lifting of hulls and modules
- Lifting of underwater equipment
- Lifting operations and relocation of Jacket/deck and floatover installation

- Offshore crane operations
- Floatover installation / removal of the hull
- Transportation (towing) of tension leg platform and the concrete substructure of such tug
- Up-ending construction
- towing

SIMA workbench supports the entire process from definition of simulation and execution for interpretation and documentation of results. It saves time by visualizing the models, giving continuous validation feedback and assistance during modeling in SIMA. In order to understand the theoretical basis of SIMA better, some characteristics are explained in the following sections.

4.2 SIMA characteristics

4.2.1 Coordinate system

There are three kinds of coordinate systems applied in SIMA which follow orthogonal and right-handed principles. They are:

- Global coordinate system, XG
- Local body fixed coordinate system, XB
- Local strip coordinate system, XS

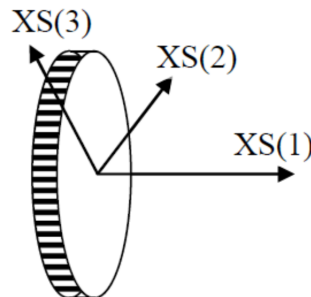


Figure 4.1: Local strip coordinate system, XS

Figure 4.1 defines a local strip coordinate system. The $XS(1)$ -axis applies to the longitudinal direction of the strip as well as the element. The $XS(2)$ -axis exists in the local strip XY plane and is perpendicular to the $XS(1)$ -axis and the $XS(3)$ is given by the orthogonal and right-handed principles.

In Figure 4.2, the local coordinate system of the slender element is defined. $[XREF, YREF, ZREF]$ defines the direction of the slender element. This reference point is an arbitrary point in the local XY -plane off the X -axis which passes through the start point and end point of the slender element and it is used to defined the direction of the positive Y -axis(5). Meanwhile, the Z -axis are given by the principle of orthogonal and right-handed.

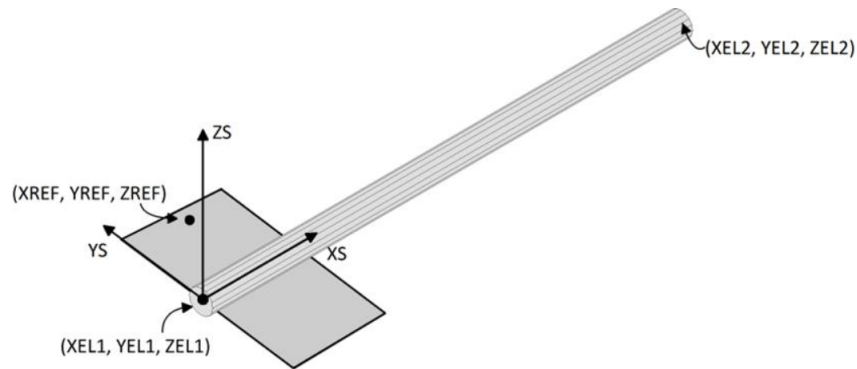


Figure 4.2: Coordinate system $[XS, YS, ZS]$ of the slender element(5)

4.2.2 Unit and physical constraints

All input data applied in SIMA must be provided in a consistent set of SI units, which are given in Table 4.1. Angles are given in degrees, [deg], and coefficients which are multiplied with rotational state variables are given for rotations in radials. Angular velocity is given in radials per time unit, for instance [rad/s]. Thruster speed and rotation are given in revolutions per minute, [RPM]. Internally in the program, all angles and rotations are converted to radials(5).

Table 4.1: Input data units set

	Property	Notation	Example
Basic Units	Length	L	m
	Time	T	s
	Mass	M	Mg=Tonne
Derived Units	Force	$F=ML/T^2$	$Mgm/s^2 = kN$
	Pressure	$P=F/L^2$	$kN/m^2=kPa$
	Velocity	$V=L/T$	m/s
	Acceleration	$A=V/T$	m/s^2

4.2.3 Coupling specifications

There are 10 types of coupling specification in SIMA, which are:

- Simple wire coupling
- Multiple wire coupling
- Lift line coupling
- Fixed elongation coupling
- Docking cone coupling
- Fender coupling
- Bumper element coupling
- Ratchet coupling
- Moment coupling
- External coupling

In this master thesis, only "simple wire coupling" and "fixed elongation coupling" are applied to model the lift wires and passive heave compensator which will be explained in Chapter 5.

Simple wire coupling

The simple wire coupling is modelled as a linear spring with effective axial stiffness $k=EA$, assuming connection flexibility is zero, where E is the modulus of elasticity and A is the cross-section area.

Fixed elongation coupling

This coupling is defined with different stiffness for different elongation range. As a result of that, it is applied to model the passive heave compensator as a spring with different stiffness when lowering into seabed and penetrating into soil.

Chapter 5

Modelling components in SIMA

5.1 Introduction of the model in SIMA

A model that can be used to evaluate the lift operation responses and as basis for case studies is established in SIMA. The modelling data are provided by co-advisor Peter Sandvik, Marintek and some of them are modified after the discussion with him. The model is made up of ship, cranemaster, hook, manifold, mudmats and the connections between them. In this chapter, all these components will be introduced briefly. Figure 5.1 shows part of the model in SIMA generally.

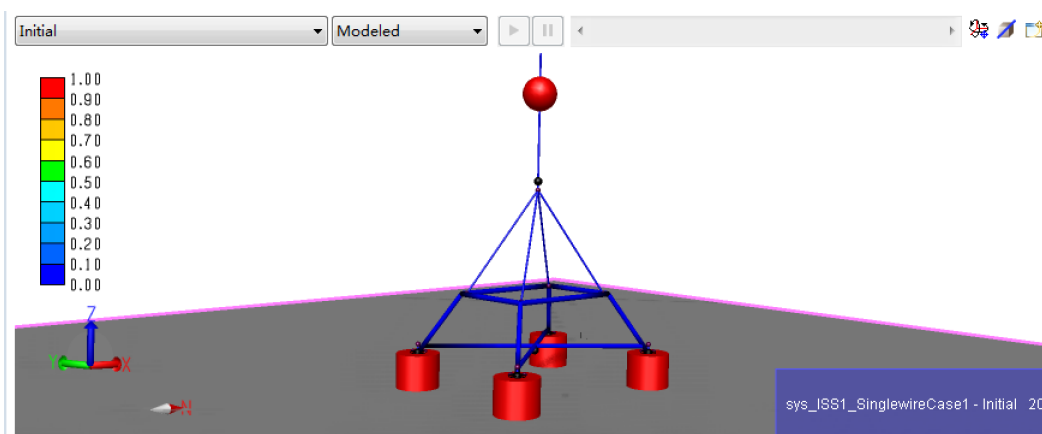


Figure 5.1: Part of the model in SIMA

The body weights of the model are presented in table 5.1.

Table 5.1: The body weights of the model in SIMA

Body	Ship	Cranemaster	Hook	Manifold and protection structure	Mudmats
Weight[kg]	$9.0 \cdot 10^6$	$1.65 \cdot 10^4$	4000	$4.306 \cdot 10^5$	$4 \cdot 1000$

In this thesis, the model is applied in 5 different environment cases and all the models are the same except for the environment conditions. So in this chapter, model in case 1 is just taken as an example to present the modelling process.

5.2 Location modelling

In this part, the position of sea surface and flat bottom is defined. Besides, some physical constants. Figure 5.2 shows the location model in SIMA and Table 5.2 presents the physical constants used in this modelling part.

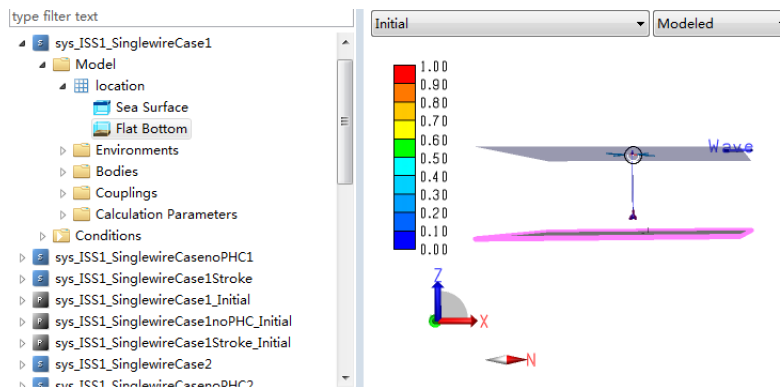


Figure 5.2: Location modelling in SIMA

Table 5.2: Physical constants in location modelling

Acceleration of gravity	Water density	Air density	Water Depth
9.81 m/s^2	1025 kg/m^3	1.25 kg/m^3	350m
Water kinematic viscosity	Air kinematic viscosity	Sea surface position	Flat bottom position
$1.188 \cdot 10^{-6} \text{ m}^2/\text{s}$	$1.824 \cdot 10^{-5} \text{ m}^2/\text{s}$	0m	-350m

5.3 Environment modelling

It is very convenient to perform the environment modelling in SIMA. There are four options to define the environment conditions in SIMA, which are:

- Wind wave
- Swell wave
- Wind
- Current

In this master thesis, only wind wave exists and the setting of case1 in SIMA is presented in Figure 5.3.

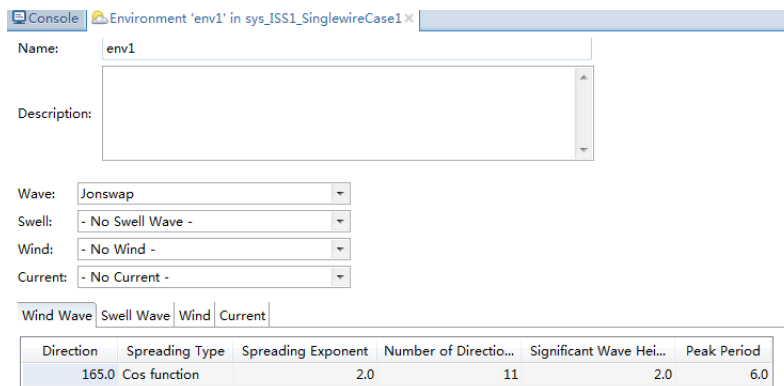


Figure 5.3: Environment modelling of case1 in SIMA

As mentioned at first of this chapter, there are 5 cases in this thesis. The characteristics of these five environment conditions are given in table 5.3.

Table 5.3: Environment conditions

Case No	Significant wave height[m]	Peak period[s]
1	2	6
2	2.5	6
3	3	6
4	2.5	8
5	2.5	10

5.4 Bodies modelling

In this section, ship, cranemaster, hook, manifold and mudmats are modelled. The modelling part contains body points, kinetics, hydrodynamic data and etc.

5.4.1 Ship modelling

The method of modelling ship in SIMA is complex. But the geometry of ship is not taken into consideration. As a result of that, it is important to define the body points which are used to connect with other bodies. Besides, a winch point is also attached to the ship which starts working at time position $t=300s$ to lower the lifting structure. Since the ship is a floating structure with large volume and weight, the body type is defined as large volume. The ship modelling and body setting are shown in Figure 5.4 and 5.5. All the kinetics data of the ship is provided by co-advisor Peter Sandvik, Marintek.

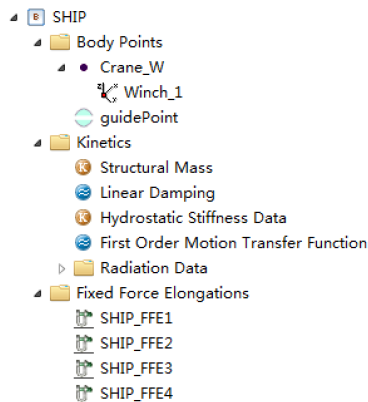


Figure 5.4: Ship modelling in SIMA

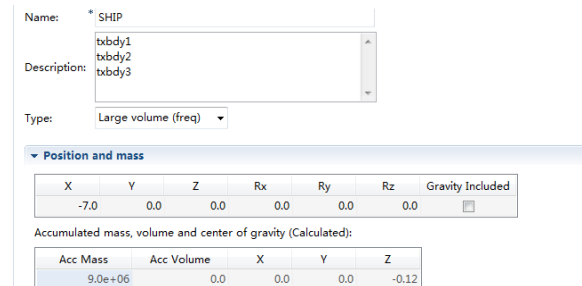


Figure 5.5: Ship body setting in SIMA

There are two points are modelled at the ship body which are winch point and guide point. The winch point is used to lower the lifting structure while the guide point is placed to change the direction of the lift wire. In addition, four fixed force elongations are defined in order to limit the horizontal motions of the ship.

5.4.2 Cranemaster modelling

The cranemaster is defined as a body with structural and added mass as well as two body points to connect the lift wire and crane wire. The upper point is connected with winch point at the ship through the guide point by lift wire. The downwards point is connected with hook by the crane wire which is modelled as the passive heave compensator. Figure 5.6 and 5.7 illustrates the detail of this part modelling in SIMA.

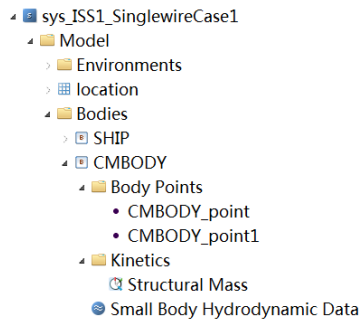


Figure 5.6: Cranemaster modelling in SIMA

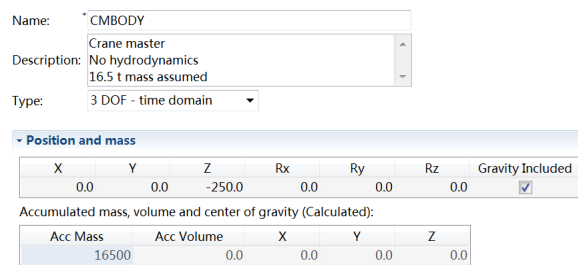


Figure 5.7: Cranemaster body setting in SIMA

5.4.3 Hook modelling

It is the same way to model hook as cranemaster in SIMA. Details about the hook modelling are illustrated in Figure 5.8 and 5.9.

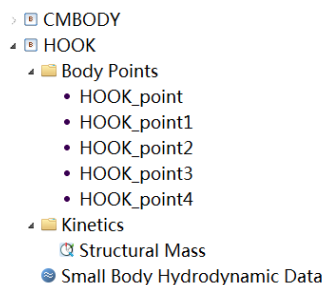


Figure 5.8: Hook modelling in SIMA

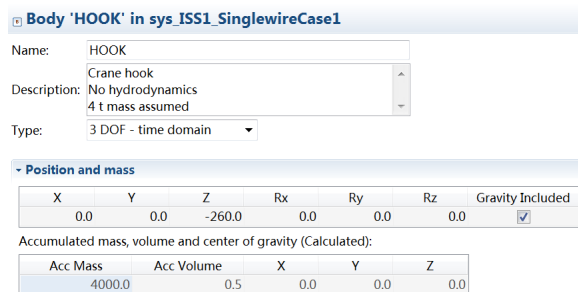


Figure 5.9: Hook body setting in SIMA

In this thesis case, the hook will be connected to four mudmats by lift wires. Therefore, it is

modelled as a body with structural and added mass as well as five points, one of which is used to connect with the downwards of the cranemaster by crane wire. Point 1 to 4 are used to connect to four mudmats.

5.4.4 Manifold and protection structure modelling

The manifold and protection structure are represented by ISS in SIMA. It is modelled as slender elements, which are blue objects shown in Figure 5.1. And the model in SIMA and body type setting is presented in Figure 5.10 and 5.11.

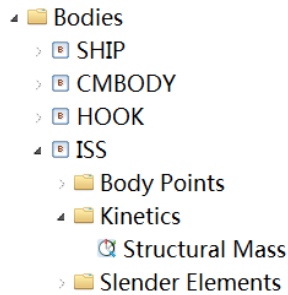


Figure 5.10: ISS modelling in SIMA

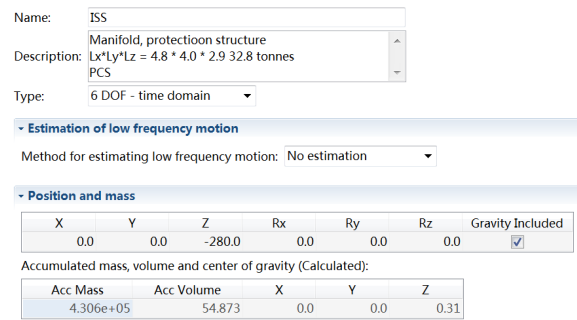


Figure 5.11: ISS body setting in SIMA

The mass and volume of this part is very large, thus it is defined as large volume structure. Then the buoyancy can be regarded as provided by these slender elements. The volume of displacement caused by slender elements can be calculated from mass divided by density of it.

Specific volume and distributed mass in SIMA represents the unit volume and mass of the slender per meter length. The specific volume is equal to the value that distributed mass divided by the density of it, which is 7850 kg/m^3 , the density of steel. There are 14 slender elements in this part and the buoyancy is provided by the total volume of displacement caused by every slender. It is the same way to model every slender of the manifold and protection structure part.

After all the slender elements defined, the buoyancy can be calculated from the equation below:

$$F_b = \rho_s \cdot V_s \cdot g \quad (5.1)$$

where F_b is the buoyancy force caused by the slender elements [N], ρ_s is the density of sea water [kg/m^3], V_s is the volume of displacement caused by all the slender elements [m^3], and g is the acceleration of gravity, which is equal to 9.81 [N/kg].

In this thesis, ISS slender element 1 is taken as an example. Figure 5.12 illustrates how it is defined.

Name: ISS_SE1

Description: Slender elements:
legs, top frame, buckets and centre unit

Wave Integration Method: Actual wave elevation

Load Type: Gravity and buoyancy included

Wave Particle Method: Velocity and acceleration

Specific Volume	Distributed Mass	Number Of Strips
0.178	1400.0	3

Calculated values

Center of gravity (calculated):

Mass	Length	Volume	X	Y	Z
14000	10.0	1.78	7.07	0.0	6.93

Coordinates

End point 1:

X1	Y1	Z1
7.07	-5.0	6.93

End point 2:

X2	Y2	Z2
7.07	5.0	6.93

Reference point:

X-Ref	Y-Ref	Z-Ref
8.07	-5.0	6.93

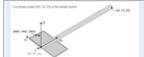


Figure 5.12: ISS Slender element 1 in SIMA

The volume of displacement caused by all the slender elements V_s can be read from Figure 5.11, which is 54.873 [m^3] and the density of sea water is 1025 [kg/m^3]. As a result of that, the buoyancy is equal to $5.52 * 10^3$ [N].

5.4.5 Mudmat modelling

There are four mudmats in this case which are the same except for the location. They are located front and aft of the starboard and port, which represented by FS, FP, AS and AP. The dimension

of each mudmat is defined as a cylinder with length of 4m and radius of 2.5m. In this thesis, mudmat FS is taken as an example to show how mudmat is modelled in SIMA. The mudmat modelling and body type setting in SIMA is illustrated in Figure 5.13 and 5.14.

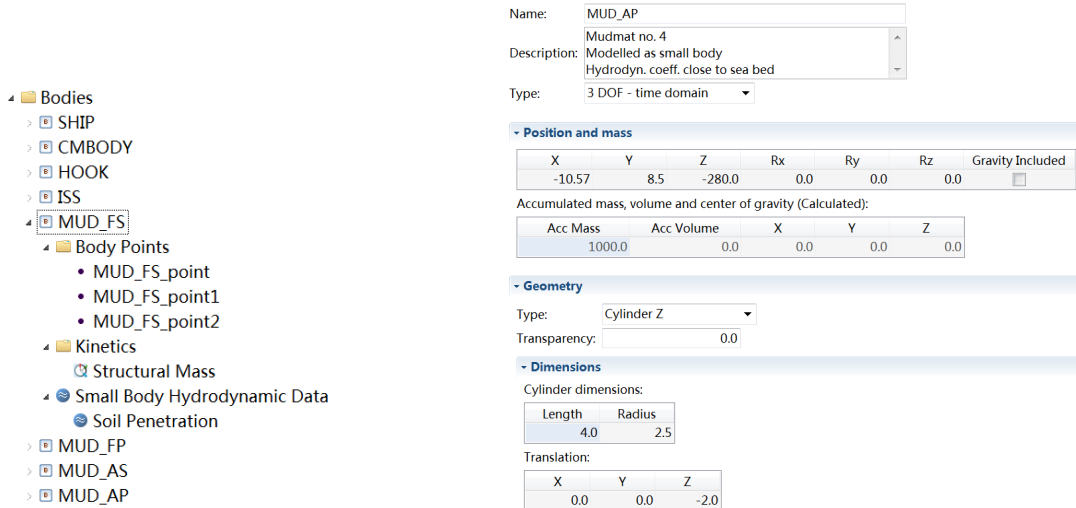


Figure 5.13: Mudmat FS modelling in SIMA Figure 5.14: Mudmat FS body setting in SIMA

The hydrodynamic coefficients is defined by quadratic term in this case. And when it starts entering into seabed, the hydrodynamic coefficients will be depth-dependent. All the data is given by Peter Sandvik, Marintek, which is based on the real case in industry field and DNV-RP-H103. the detail will be illustrated in Figure 5.15.

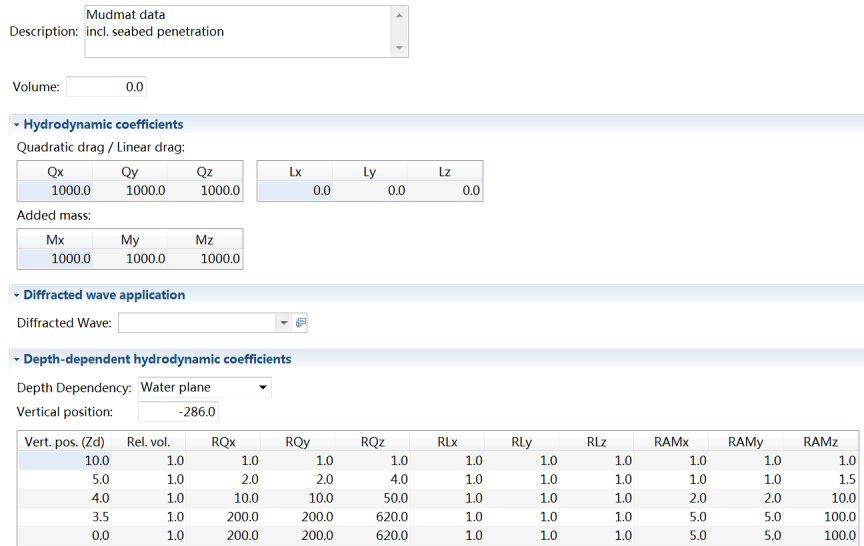


Figure 5.15: Hydrodynamic data on Mudmat FS in SIMA

The vertical position in Figure 5.15 is where the first contact between mudmats and seabed

happens, which is -286 m.

When mudmat penetrates into seabed, there is friction force for both upward and downward motions which is dependent on the depth of mudmat. The penetration is related to the first contact depth. The data is also provided by Peter Sandvik, Marintek. Figure 5.16 presents the detail of soil penetration forces modelling on mudmat FS in SIMA.

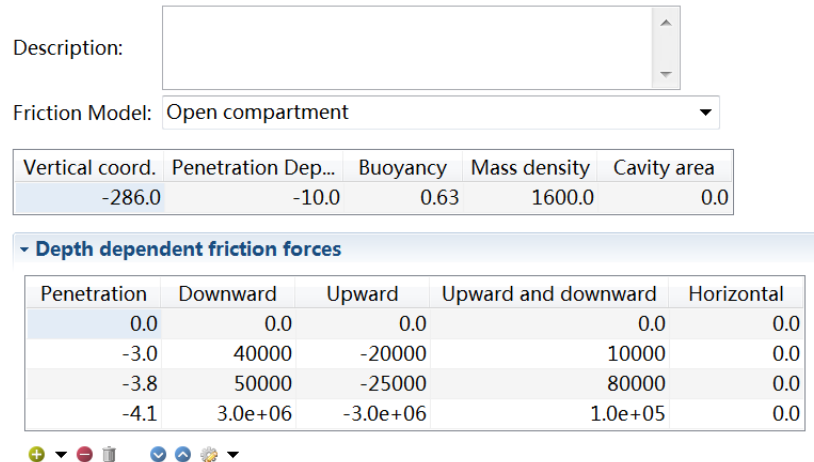


Figure 5.16: Soil penetration on Mudmat FS in SIMA

The other three mudmats are modelled in the same way as Mudmat FS which is given in this section.

5.5 Coupling modelling

There are 10 types of coupling specification in SIMA, which are given in chapter 4.2.4. And in this thesis, only simple wire couplings and fixed elongation couplings are applied. Lifting wires and crane wires play an important role in the whole model. Therefore the coupling modelling will determine the performance of the heavy lifting operation. The following table presents the end points and coupling type of all the wires in this case.

Table 5.4: End points and types of the wires

Wire names	End points	Coupling types
Sling FS	The hook and mudmat FS	Simple wire coupling
Sling FP	The hook and mudmat FP	Simple wire coupling
Sling AS	The hook and mudmat AS	Simple wire coupling
Sling AP	The hook and mudmat AP	Simple wire coupling
Lifting wire	The winch and the hook	Simple wire coupling
Crane wire	The crane master and the hook	Fixed elongation coupling
Crane wire measurement	The crane master and the hook	Fixed elongation coupling

5.5.1 Simple wire couplings

The sling and the lifting wire are defined as simple wire couplings. There are four slings connected the hook to the four mudmats respectively and one lifting wire connected between the winch and crane master through the guide point at the ship in this case. In SIMA, the length of the wire can be calculated after giving the two end points. Then, the proprieties for the wires are defined in SIMA. Since it is assumed that no failure or break happens, the connection flexibility is zero in this case. Besides, the material damping is assumed around 10% of wire cross section stiffness which is provided by Peter Sandvik, Marintek. The four slings are modelled in the same way, thus only the modelling of one sling between hook and mudmat FS is presented in Figure 5.17.

Name: SLING_FS

Description:

Length	Flexibility	Damping	Ea	Failure Mode	Breaking Strength	Failure Time
14.5	0.0	1.8e+06	2.0e+08	None	0.0	0.0

▸ Calculated values

▾ Body points:

End point 1	Body 1	End point 2	Body 2
HOOK_point1	HOOK	ISS_point	ISS

▾ Guide points:

Guide Point	Entered On Line

+ - 🗑️ 🔄 📄 📄

Figure 5.17: Sling FS modelling in SIMA

The lifting wire is modelled in the same way as slings and the only difference is the wire cross section stiffness data. The detail information about lifting wire will be illustrated in Figure 5.18.

Name: *LIFTW

Description:

Length	Flexibility	Damping	Ea	Failure Mode	Breaking Strength	Failure Time
264.39	0.0	3.0e+06	3.2e+08	None	0.0	0.0

▶ Calculated values

▼ Body points:

End point 1	Body 1	End point 2	Body 2
Crane_W	SHIP	CMBODY_point1	CMBODY

▼ Guide points:

Guide Point	Entered On Line
guidePoint	<input checked="" type="checkbox"/>

+ ▼ - ☒ ↻ ↺ ↻ ▼

Figure 5.18: Lifting wire modelling in SIMA

5.5.2 Fixed elongation coupling

As presented in Table 5.4, the crane wire and crane wire measurement are defined as fixed elongation coupling in this case. It is a different way to define the wire with simple coupling modelling. In this type of coupling, the force elongation relationship is defined. The relationship curve is not necessary to be a straight line with a single stiffness. It can be different curves for different elongation range. And the damping is defined as a proportional component to an exponent of the velocity.

Meanwhile, this type of coupling is also applied to restrict the relative three-dimension motions between the mudmat and slender elements. There are 12 fixed elongation coupling restriction modelling in this case. All the restriction is modeled as a spring with no failure or break mode. And all the damping and force parameters are defined with the same linear interpolation in each mudmats as well as X, Y and Z direction. The restriction modelling of mudmat FS in X-direction is illustrated in Figure 5.19.

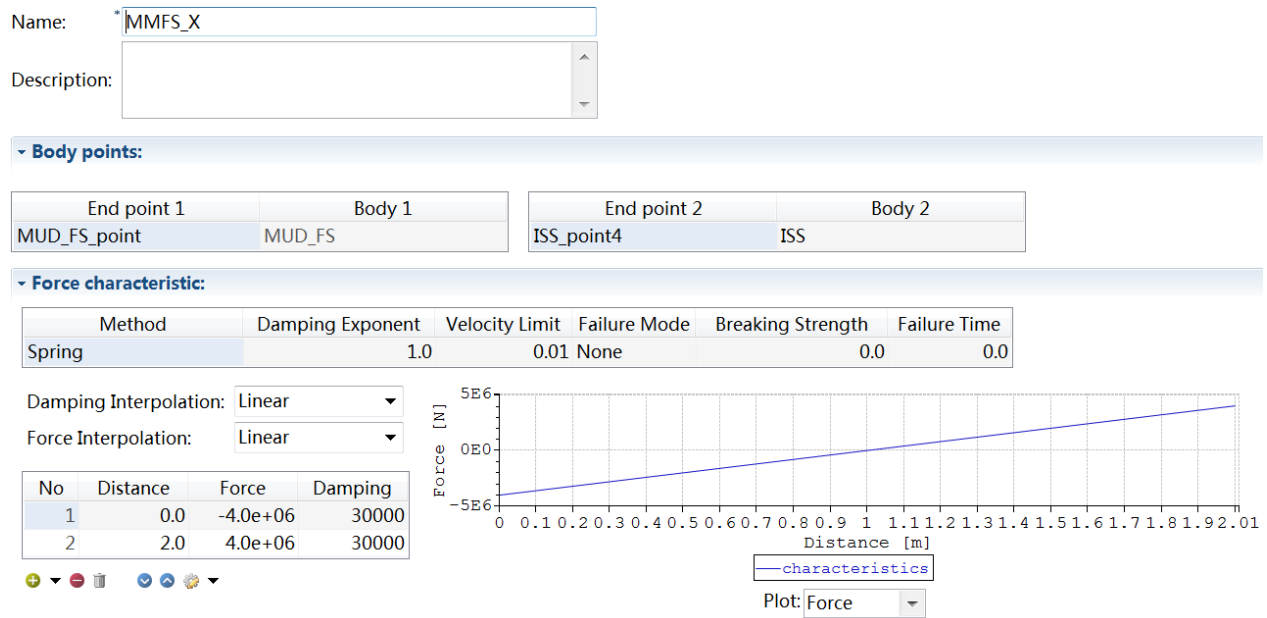


Figure 5.19: Restriction modelling of mudmat FS in X-direction in SIMA

It is also obvious that the crane wire and crane wire measurement have the same end points and coupling type characteristics.

The crane wire is placed between the hook and crane master. The method for initialization of coupling element is spring and the crane wire model is shown in Figure 5.20.

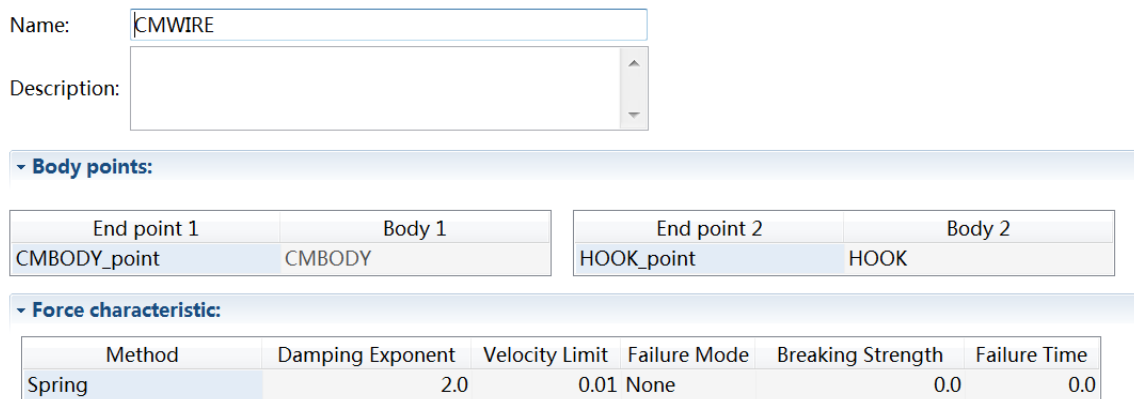


Figure 5.20: Crane wire modelling in SIMA

In the crane wire modelling, both of the force and damping interpolation are linearly defined with three curves, which stand for the process of lowering into seabed, penetrating into seabed with the influence of passive heave compensator and stopping. The initial stroke is assumed

to be from 7m to 13m with the equilibrium at distance of 10m, which is the initial length of the crane wire. The coupling force at the equilibrium position can be calculated by the vertical force equilibrium equation of the whole underwater system.

$$F_e = Mg - F_b \tag{5.2}$$

where F_e is the coupling force at the equilibrium position [N], M is the total mass of underwater structure, F_b is the buoyancy force caused by the slender elements [N], which is calculated in chapter 5.4.4, and g is the acceleration of gravity, which is equal to 9.81 [N/kg]. The crane wire force and damping interpolation are illustrated in Figure 5.21 and 5.22.

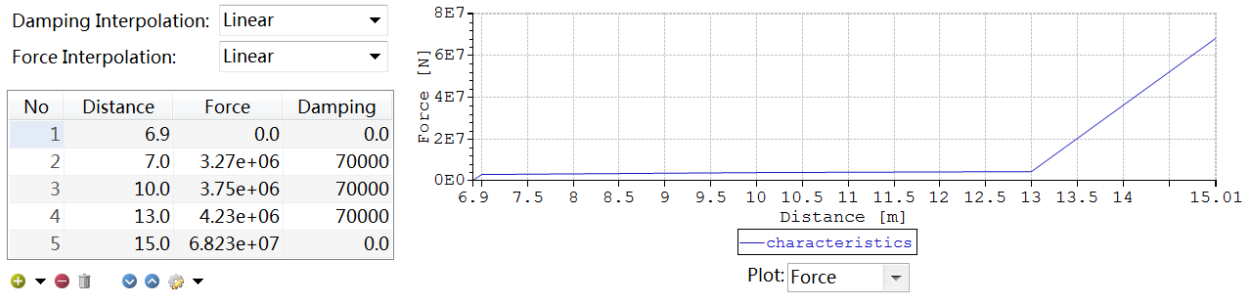


Figure 5.21: Force interpolation of crane wire in SIMA

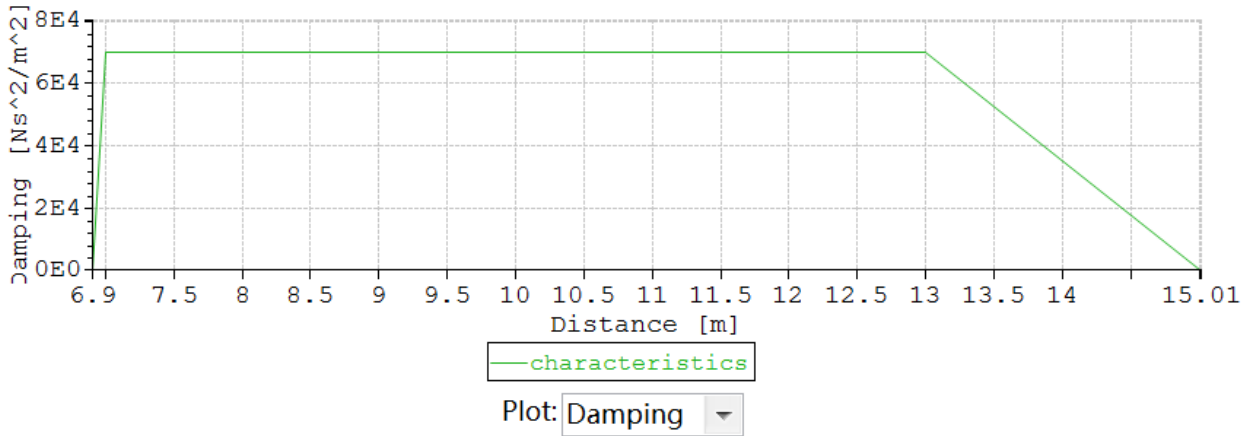


Figure 5.22: Force interpolation of crane wire in SIMA

It is presented obviously that the wire force is zero when the wire length is shorter than 6.9m in Figure 5.21. Meanwhile, the wire force will increase immediately to a certain value within a very little elongation of 0.1m and then it will vary slowly within the assumed stroke range from 7m

to 13m, which represents that the passive heave compensator starts working so that the tension force of the wire remains a relative steady level inside the stroke length. After the stroke range, the wire force will increase as fast as it behaves between 6.9m to 7m.

The crane wire measurement is defined similar with the crane wire but the force interpolation is linear with a slop of 1N/m thus the elongation is equal to the coupling force, which makes it more convenient and simple to obtain the elongation of the crane wire through the force varied range in the crane wire measurement. This will be used to optimize the stroke afterwards. Figure 5.23 illustrates the crane wire measurement modelling in SIMA, which is represented by CMMEAS.

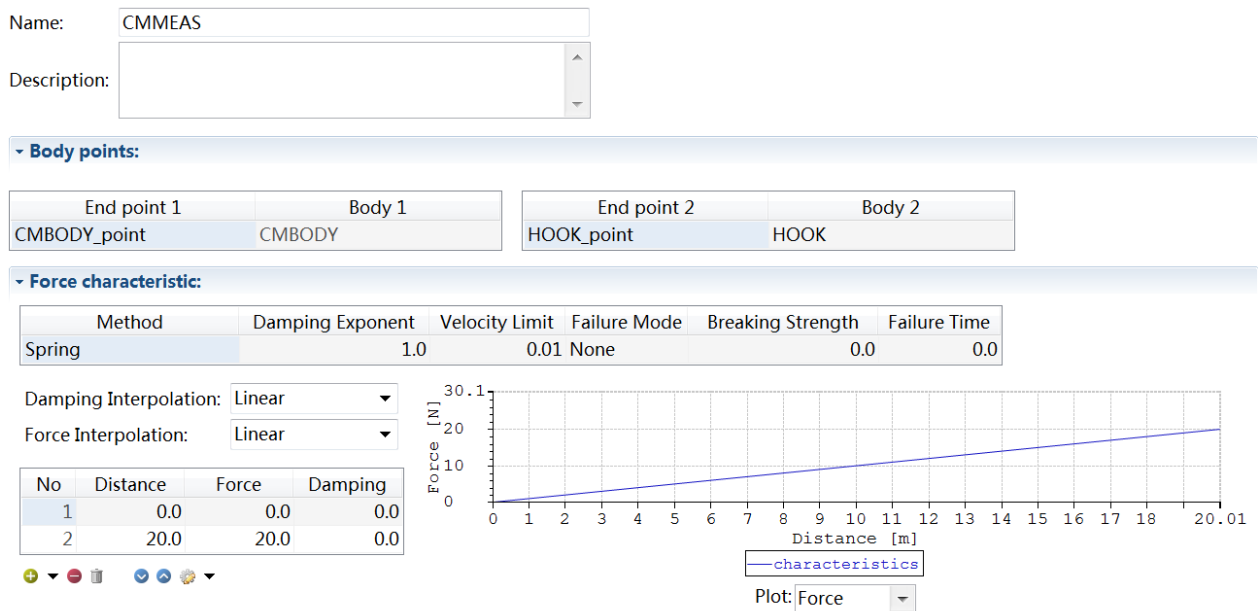


Figure 5.23: Crane wire measurement modelling in SIMA

As for the model without passive heave compensator, the crane wire with fixed elongation coupling is modified with simple wire coupling.

5.6 Calculation parameters modelling

The SIMA program provides two types of calculation: static and dynamic calculation. The related parameters and procedure of each calculation are defined in this part.

5.6.1 Static calculation modelling

The static calculation parameters are:

- Maximum natural period
- Position tolerance
- Direction tolerance
- Equilibrium time step
- Maximum number of time steps

Figure 5.24 shows how the static calculation defined in SIMA.

Run Static Automatically:

Calculate Equilibrium:

Calculate Eigenvalues:

Write Visualization File:

Multiple Equilibrium Calculations:

Equilibrium Calculation Method:

Max Period	Pos Tol	Dir Tol	Time Step	Max Step	Critical Damping
10.0	0.1	0.1	0.001	1000000000	<input checked="" type="checkbox"/>

[set to SIMO default](#) [set to MOP default](#)

Figure 5.24: Static calculation modelling in SIMA

What is important in this part is that the maximum natural period and equilibrium should be defined properly. The maximum natural period acts as the maximum limit value to find the natural period of the structure. If it is too small, the natural period can not be find within the limit value. However, it will take too much time to run the static analysis if the value is too large. As for the equilibrium time step, it is a strategy to use the minimum value of SIMA can provide to ensure that the calculation can be done.

5.6.2 Dynamic calculation modelling

There are general sand storage setting in dynamic calculation modelling. What should be paid attention to is the simulation length and time step setting. Since the winch is set to start at 100s

General Storage

Simulation Length	Time Step
600.0	0.005

Time series generation parameters

Wave Seed	Wind Seed
1	1

Requested Time Series Length	Time Increment	Applied Time Series Length	Frequency Resoluti...	Number Of Steps
600.0	0.005	655.36	0.0015259	131072

Figure 5.25: General dynamic calculation modelling in SIMA

General Storage

The time increment for storage is equal to the time increment for time series generation, which is: 0.005

Write visualization file:

Store Wind Forces:	<input type="checkbox"/>	Store Sum Specified Forces:	<input checked="" type="checkbox"/>
Store Total Forces:	<input type="checkbox"/>	Store Sum External Forces:	<input type="checkbox"/>
Store Retardation Forces:	<input type="checkbox"/>	Store Sum Coupling Forces:	<input checked="" type="checkbox"/>
Store Hydrostatic Stiffness Forces:	<input type="checkbox"/>	Store Resultant Coupling Element Forces:	<input checked="" type="checkbox"/>
Store Linear Damping:	<input checked="" type="checkbox"/>	Store Global Coupling Force Components:	<input checked="" type="checkbox"/>
Store Quadratic Damping:	<input checked="" type="checkbox"/>	Store Local Coupling Force Components:	<input checked="" type="checkbox"/>
Store Distributed Hydrodynamic Forces:	<input checked="" type="checkbox"/>	Store Global Low Frequency Position:	<input type="checkbox"/>
Store Wave Drift Damping:	<input checked="" type="checkbox"/>	Store Global Total Position:	<input checked="" type="checkbox"/>
Store Linear Current Drag:	<input checked="" type="checkbox"/>	Store Global Acceleration:	<input checked="" type="checkbox"/>
Store Quadratic Current Drag:	<input checked="" type="checkbox"/>	Store Local Velocity:	<input checked="" type="checkbox"/>
Store Small Body Hydrodynamic Forces:	<input checked="" type="checkbox"/>		
Store Resultant Positioning Element Forces:	<input type="checkbox"/>		
Store Positioning Element Force Components:	<input type="checkbox"/>		
Store Total Positioning Forces:	<input type="checkbox"/>		
Store Thruster Forces:	<input type="checkbox"/>		
Store Sum Thruster Forces:	<input type="checkbox"/>		
Store Dynamic Positioning Estimators:	<input type="checkbox"/>		

[store everything](#) [store nothing](#)

Figure 5.26: Storage information of the dynamic calculation in SIMA

and stop at 600s when modelling the ship, the simulation length is consistent with it. And the time step should not be too large or too small thus it is 0.005s in this case. Figure 5.25 illustrates the general setting of dynamic calculation.

Moreover, the demanded data are chosen to be stored in the storage setting. And the time increment for storage is equal to the time increment for time series generation which is 0.005s in this case. In this thesis, It is presented in Figure 5.26.

This chapter gives a detail introduction of how the different components are established in SIMA program, including environment, location, bodies, couplings and calculation parameters modelling.

After defining all the calculation parameters in SIMA, the model is finally established. And the other models with different environment conditions can be established in the same way. In the next chapter, the static and dynamic analysis will be carried out and the results will be presented.

Chapter 6

Results and analysis

6.1 Static Analysis

As soon as the static analysis is carried out, the results file will be generated in SIMA, which contains the static equilibrium position and different types of forces.

Table 6.1 will present the static body position of all the underwater structure.

Table 6.1: Static body positions of underwater structures

Body	X[m]	Y[m]	Z[m]	Rx[Deg]	Ry[Deg]	Rz[Deg]
Crane master	0.01	0.00	-253.48	0.00	0.00	0.00
Hook	0.01	0.00	-262.97	0.00	0.00	0.00
Mudmat FS	10.58	-8.50	-283.13	0.00	0.00	0.00
Mudmat FP	10.58	8.50	-283.13	0.00	0.00	0.00
Mudmat AS	-10.57	-8.50	-283.13	0.00	0.00	0.00
Mudmat AP	-10.57	8.50	-283.13	0.00	0.00	0.00

In order to compare the static vertical position with the initial vertical position, the initial position and the deviation will be given in Table 6.2.

Table 6.2: Vertical positions deviation

Body	Crane master	Hook	Mudmat FS	Mudmat FP	Mudmat AS	Mudmat AP
Initial Z-pos[m]	-250.00	-260.00	-280.00	-280.00	-280.00	-280.00
Static Z-pos[m]	-253.48	-262.97	-283.13	-283.13	-283.13	-283.13
Deviation	-3.48	-2.97	-3.13	-3.13	-3.13	-3.13

These negative deviations in Table 6.2 describe that all the structures move downwards around 3m when the static analysis is performed.

In addition, the coupling force components in the lifting and crane wire will be presented in Figure 6.3.

Table 6.3: Coupling forces and moments in wires

Wire name	Ftotal[N]	Fx[N]	Fy[N]	Fz[N]	Mx[Nm]	My[Nm]	Mz[Nm]
Lifting wire	3.83E+06	3.49E+02	-6.69E-03	3.83E+06	0.00	3.00	0.00
Crane wire	3.67E+06	-3.39E+02	6.17E-03	-3.67E+06	0.00	0.00	0.00

The results in Table 6.3 are read from the wire forces connected to crane master. It is the same as the results read from the wire forces connected to the other end structure except the opposite direction of vertical forces.

6.2 Dynamic Analysis

The dynamic analysis is carried out after the static analysis is done. At first, some basic information should be provided.

When the winch point is defined at the ship modelling part, it is set to start working at time $t=100s$ with velocity of $0.1m/s$ and stop at time $t=600s$. Since we know the static equilibrium position of mudmat from table 6.1 as well as the length of the mudmat is $4m$, and the first contact happens at vertical position $Z=-286m$, the first contact time can be calculated, which is $t=109s$. Some related information will be presented in Table 6.3.

Table 6.4: Related information about dynamic analysis

Winch starts time[s]	First contact time[s]	Analysis stops time[s]
100	109	600
Mudmat length[m]	First contact position[m]	Max penetration length[m]
4	-286	10

6.2.1 Dynamic analysis on Mudmat

The passive heave compensator is to applied to reduce the vertical loads and motions during heavy lifting operation. In this thesis, the process of penetrating into the seabed is of focus. And in order to prove the passive heave compensator works in this process, the vertical coupling system force and velocity of the mudmat will be plotted. Mudmat FS is taken as an example and the five cases are explained in Table 5.3.

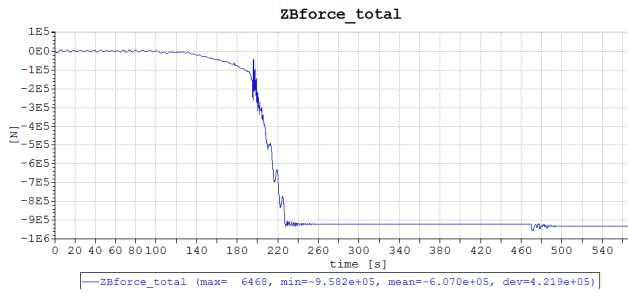


Figure 6.1: Vertical coupling force in Mudmat FS with PHC, Case 1

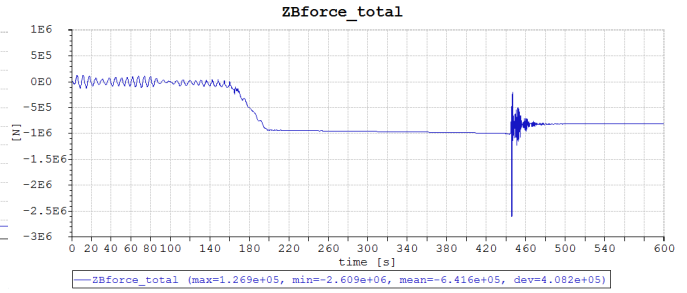


Figure 6.2: Vertical coupling force in Mudmat FS without PHC, Case 1

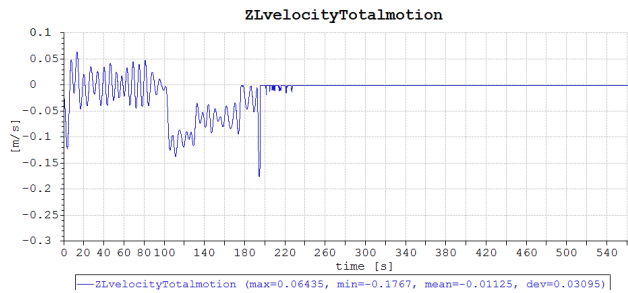


Figure 6.3: Vertical velocity of Mudmat FS with PHC, Case 1

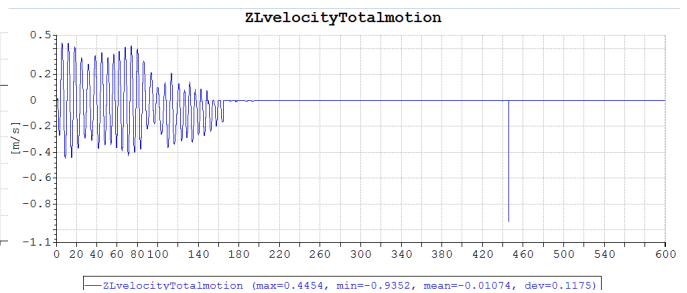


Figure 6.4: Vertical velocity of Mudmat FS without PHC, Case 1

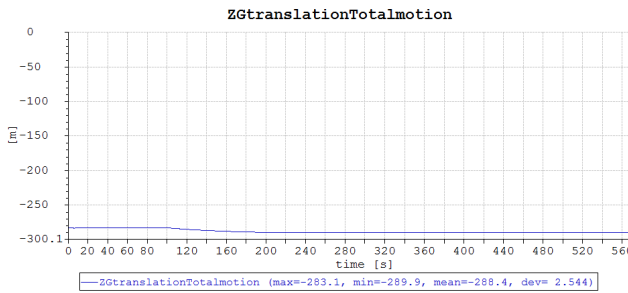


Figure 6.5: Vertical global translation of Mudmat FS with PHC, Case 1

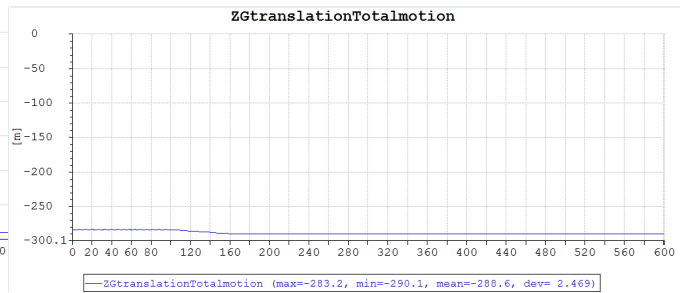


Figure 6.6: Vertical global translation of Mudmat FS without PHC, Case 1

Figure 6.1 to Figure 6.6 illustrates the vertical coupling force, vertical velocity and vertical global

translation of mudmat FS with and without PHC (passive heave compensator) in case 1. Overall, the global translation is of less concern compared with the other two parameters. Therefore, it will not be plotted in the other cases.

It has to be mentioned that there exists a sudden variation around 440s in Figure 6.2 and this might also happen in other cases. However, this is caused by the bug of SIMA program and it can't be eliminated. In order to avoid the influence of this sudden variation, the post processor is introduced in SIMA to optimize the results. Assumed that the mudmat reaches the max penetration length with a constant velocity of 0.1m/s, it will just take 100s to this penetration since the winch starts working. As a result of that, all the statistics are filtered from 0s to 400s, which is far before the sudden variation.

Regardless of the sudden variation, the dynamic results in case 1 will be listed in Table 6.5.

Table 6.5: Optimized results of Mudmat FS in case 1

Parameters		Max. value	Min. value	Mean value	Deviation
Vertical Coupling force[N]	PHC	6.47E-02+03	-9.34E+05	-4.47E+05	4.36E+05
	No PHC	1.27E+05	-9.84E+05	-5.34E+05	4.57E+05
Vertical velocity[m/s]	PHC	6.43E-02	-1.77E-01	-1.69E-02	3.66E-02
	No PHC	4.45E-01	-4.50E-01	-1.56E-02	1.42E-01

It is obvious to find that the vertical force and velocity of mudmat are alleviated when PHC is applied. As for the vertical coupling force, the maximum and mean value drop 95% and 16% respectively when PHC is used in this case while the minimum value and deviation don't change too much.

Moreover, the maximum and minimum value of vertical velocity of mudmat in case 1 is also reduced in 85% and 60% while the deviation is 75% less compared to the model without PHC.

As a result of that, it proves that the passive heave compensator can help to alleviate the vertical force and motion of the lifting template during heavy lifting operation.

The vertical coupling force and velocity of mudmat FS in case 2 to case 5 will be presented in the following Figures 6.7-6.22. And the statistics will be analyzed in the discussion section to draw the conclusion.

As for the results of the force and velocity of the other three mudmats in all the five cases will be attached to the Appendix A and B respectively.

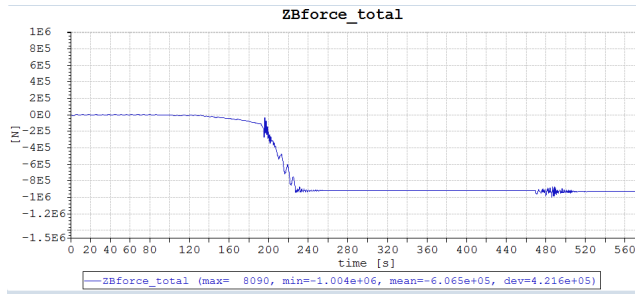


Figure 6.7: Vertical coupling force in Mudmat FS with PHC, Case2

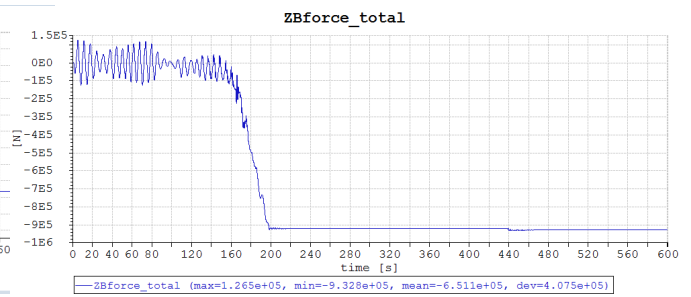


Figure 6.8: Vertical coupling force in Mudmat FS without PHC, Case2

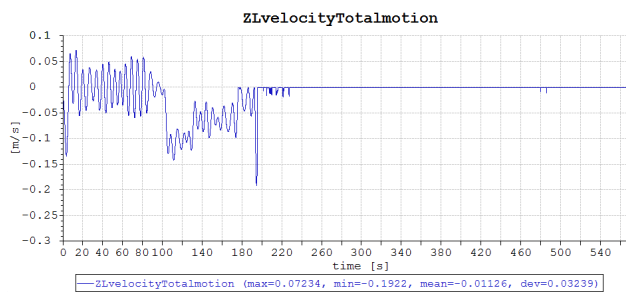


Figure 6.9: Vertical velocity of Mudmat FS with PHC, Case2

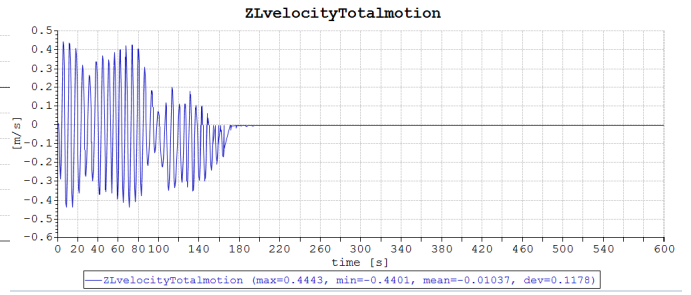


Figure 6.10: Vertical velocity of Mudmat FS without PHC, Case2

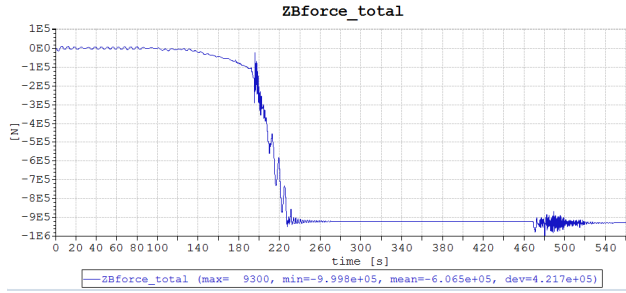


Figure 6.11: Vertical coupling force in Mudmat FS with PHC, Case3

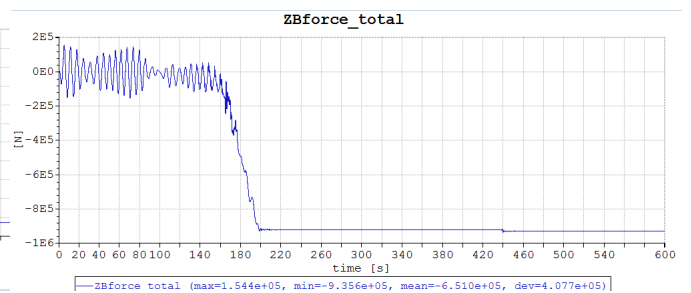


Figure 6.12: Vertical coupling force in Mudmat FS without PHC, Case3

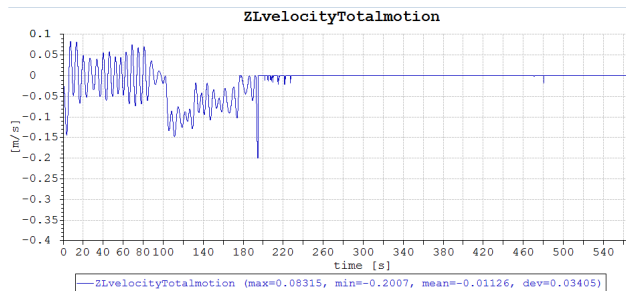


Figure 6.13: Vertical velocity of Mudmat FS with PHC, Case3

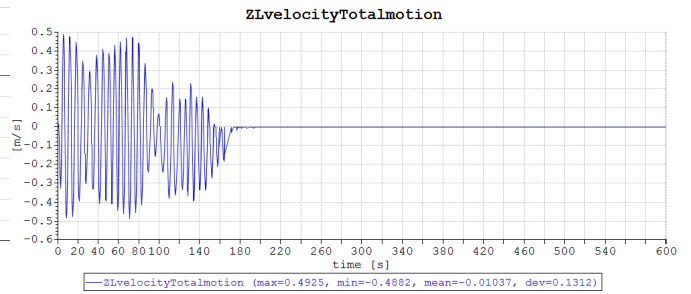


Figure 6.14: Vertical velocity of Mudmat FS without PHC, Case3

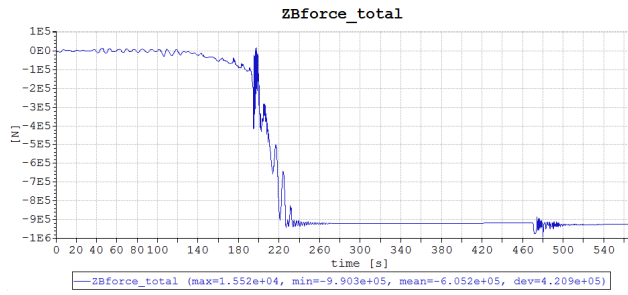


Figure 6.15: Vertical coupling force in Mudmat FS with PHC, Case4

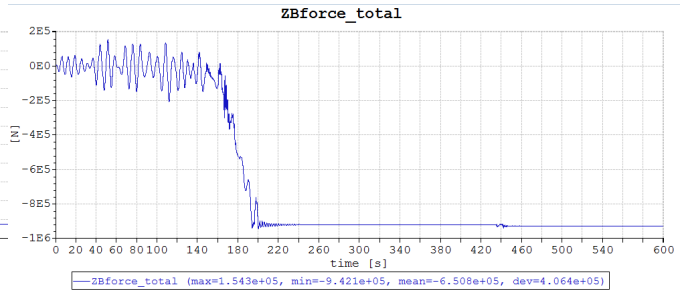


Figure 6.16: Vertical coupling force in Mudmat FS without PHC, Case4

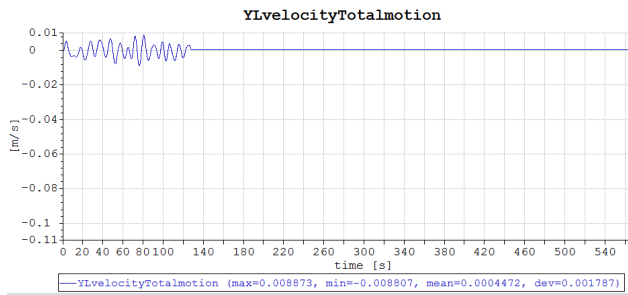


Figure 6.17: Vertical velocity of Mudmat FS with PHC, Case4

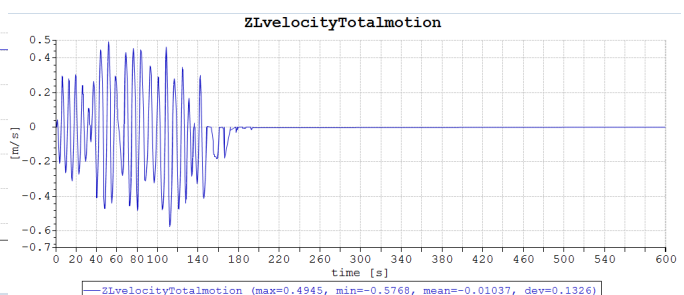


Figure 6.18: Vertical velocity of Mudmat FS without PHC, Case4

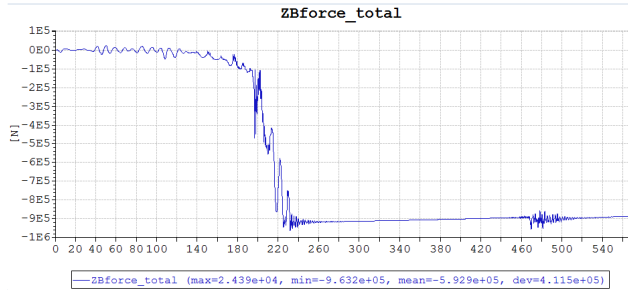


Figure 6.19: Vertical coupling force in Mudmat FS with PHC, Case5

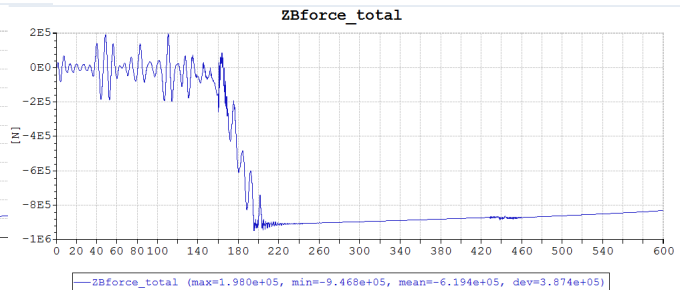


Figure 6.20: Vertical coupling force in Mudmat FS without PHC, Case5

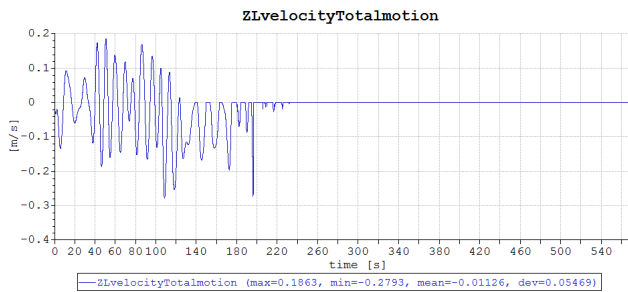


Figure 6.21: Vertical velocity of Mudmat FS with PHC, Case5

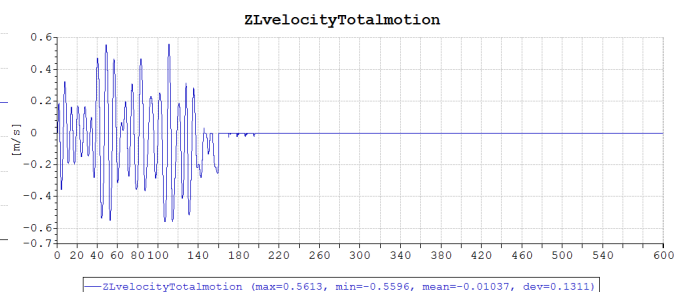


Figure 6.22: Vertical velocity of Mudmat FS without PHC, Case5

6.2.2 Dynamic analysis on Crane wire

In order to optimize the stroke of the passive heave compensator, the force in the crane wire needs to be found out. Since the crane wire is connected between the crane master and hook, the coupling system force can be read from either the result of crane master or hook. In this thesis, the statistics from the hook will be plotted.

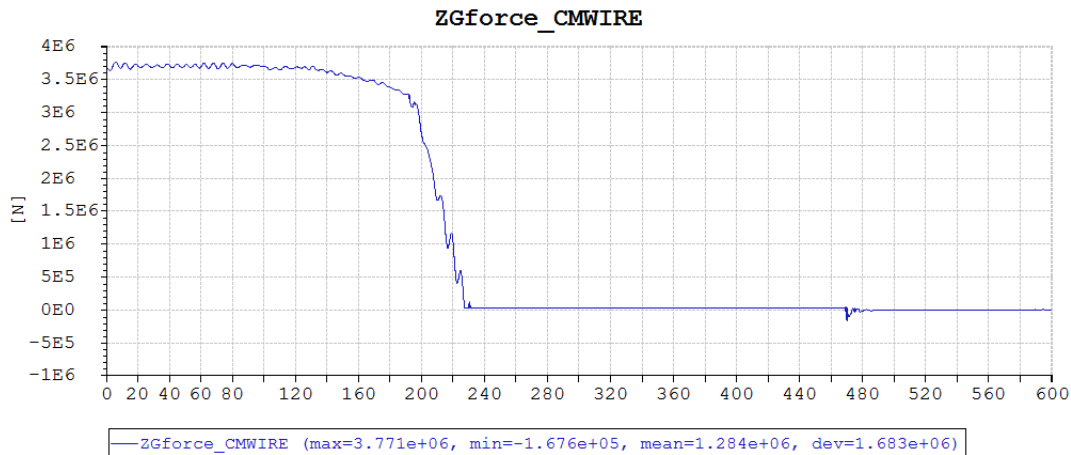


Figure 6.23: Coupling system force in crane wire, Case1

Figure 6.23 shows the coupling force in crane one during the penetrating process in case1. Similarly as what is mentioned in last section, the influence of the sudden variation can be eliminated by post processor in SIMA program. Then the maximum and minimum value of the crane wire force can be obtained, which are $3.77E+06N$ and $2.30E+04N$. And the force interpolation is provided by Figure 5.22. Then, the elongation can be calculated, which varies from 6.9m to 10.125m.

However, there is a more simple way to find the elongation by crane wire measurement. Figure 6.24 presents the coupling system force in crane wire measurement of case1.

After optimizing the result by post processor in SIMA, the maximum and minimum force in crane wire measurement is 10.1N and 6.9N. Since the stiffness of this wire is 1N/m, it's easy to obtain that the wire varies in range from 6.9m to 10.1m, which is the same as the result from the crane wire method. Considering that there exists some deviation of the results from SIMA, the optimized stroke can be defined from 6.5m to 11.0m with the equilibrium position at 10m in case1.

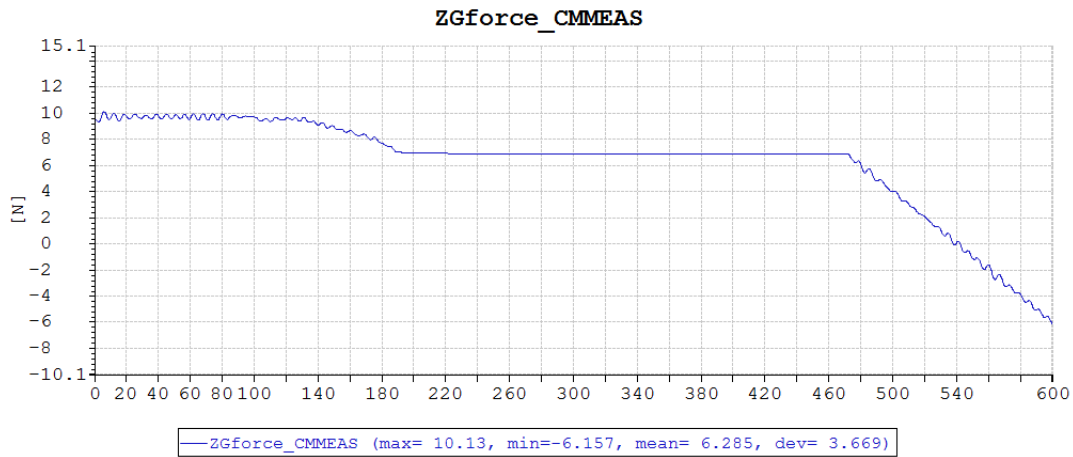


Figure 6.24: Coupling system force in crane wire measurement, Case1

In the same way the vary range of the crane wire length can be obtained from the crane wire measurement way. It will be listed in Table 6.6. Therefore, the optimized stroke of the passive

Table 6.6: Coupling system force in Crane wire measurement

Case number	Maximum value[N]	Minimum value[N]	Crane wire length vary range[m]
1	10.10	6.90	6.90-10.10
2	10.20	6.90	6.90-10.20
3	10.30	6.90	6.90-10.30
4	10.30	6.89	6.89-10.30
5	10.60	6.85	6.85-10.60

heave compensator is defined as 6.5m to 11.0m with the equilibrium length of 10m for all the five cases.

The coupling system force in both crane wire and crane wire measurement in different cases will be presented in Figure 6.25 to Figure 6.32. And the results of the passive heave compensator with optimized stroke will be illustrated in next section.

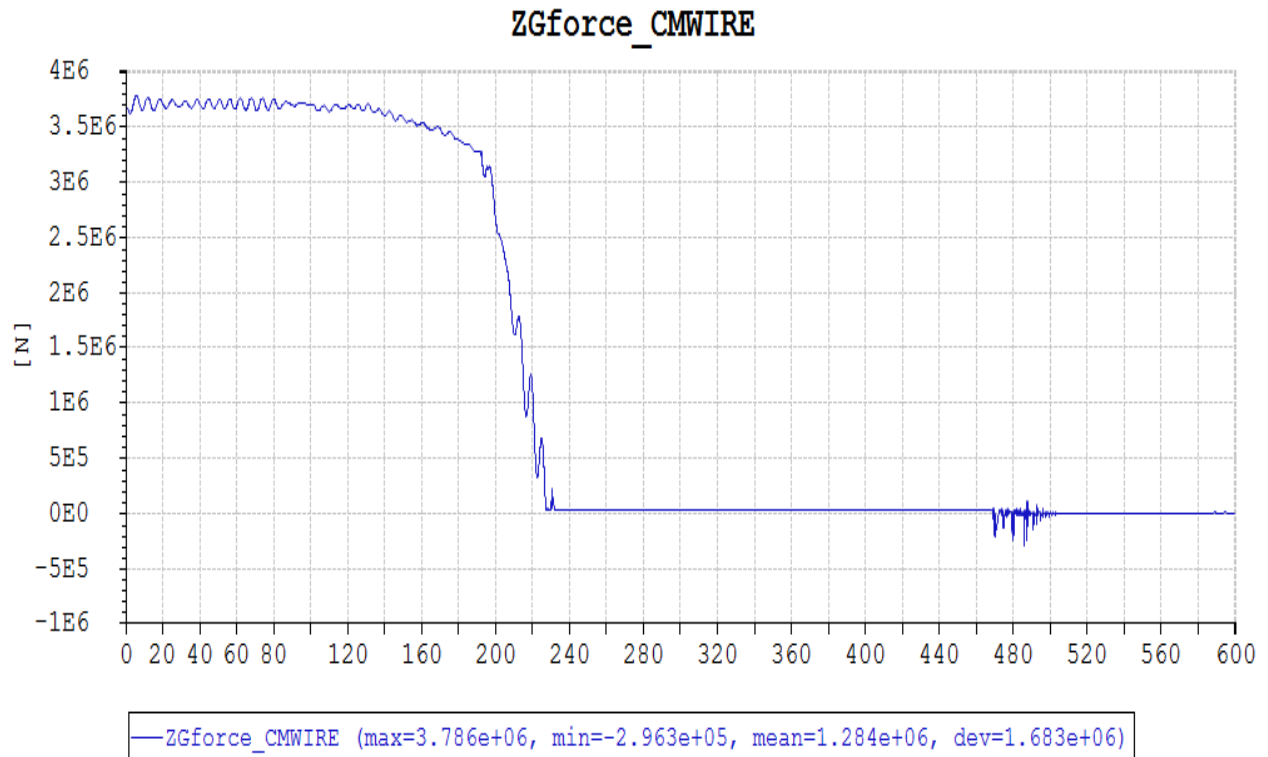


Figure 6.25: Coupling system force in crane wire, Case2

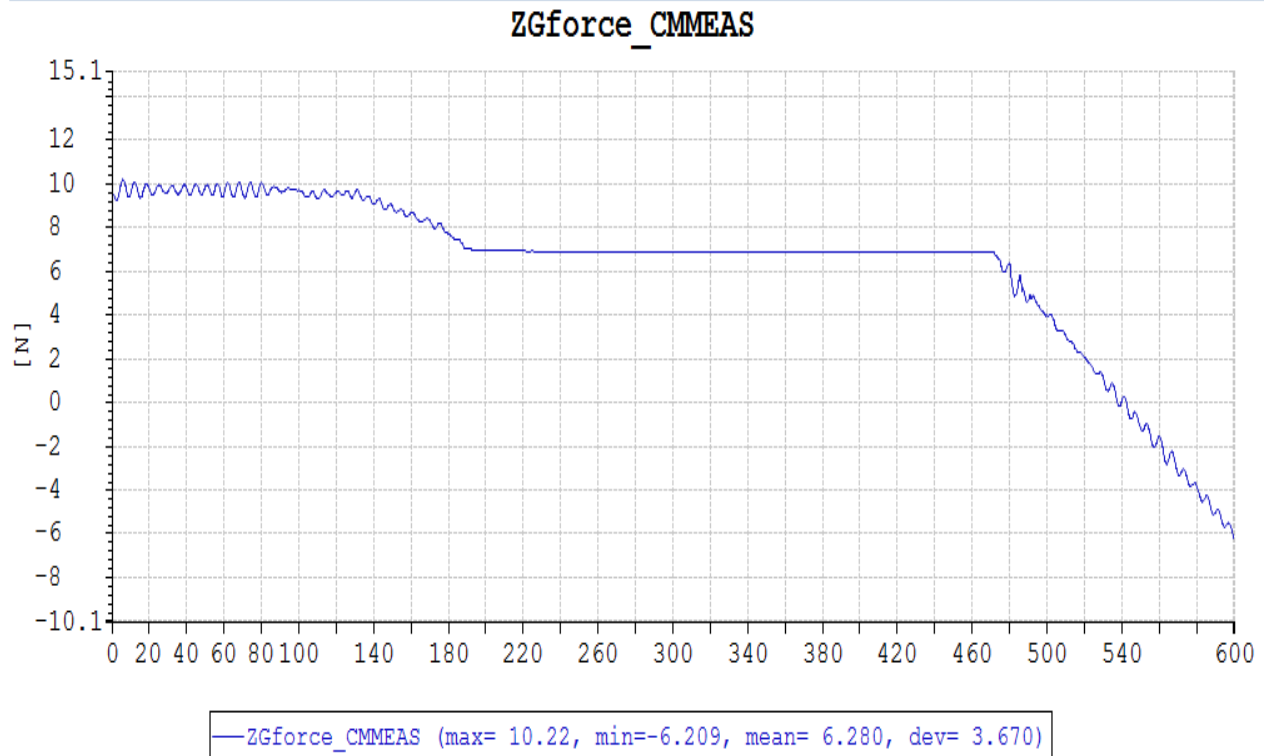


Figure 6.26: Coupling system force in crane wire measurement, Case2

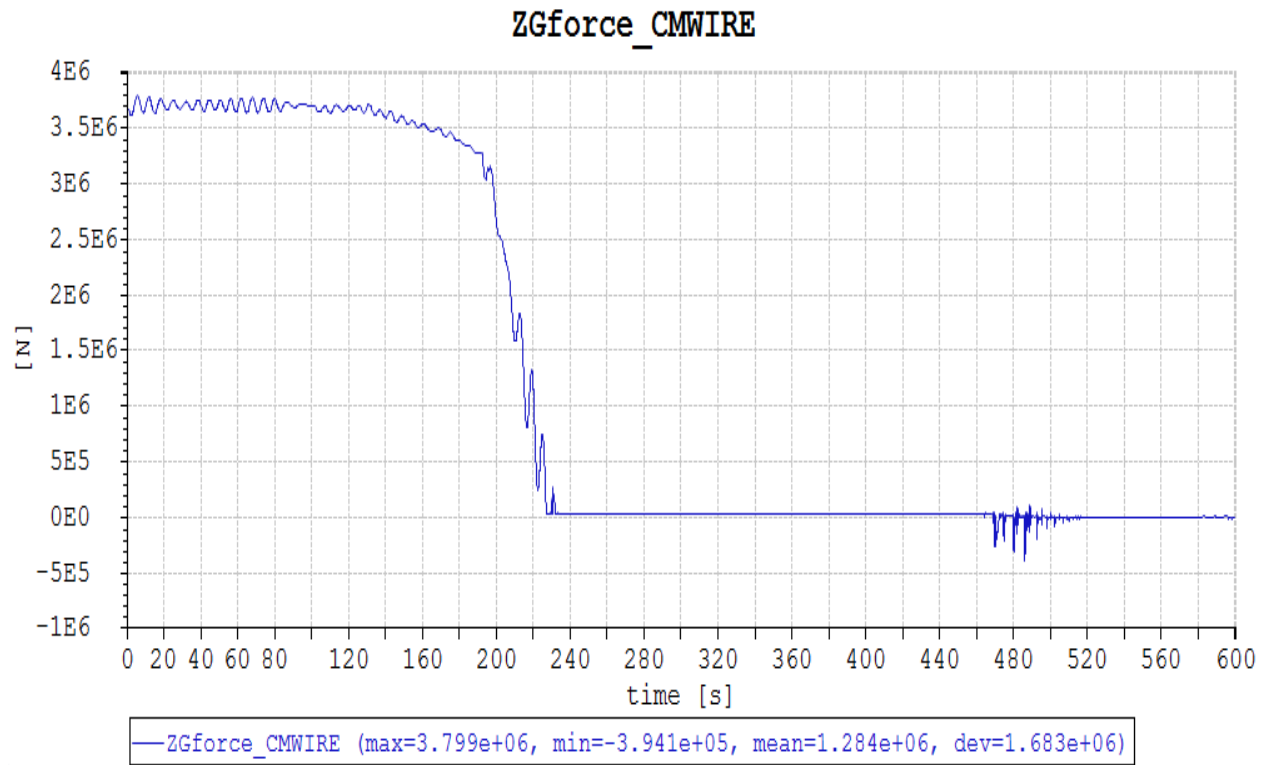


Figure 6.27: Coupling system force in crane wire, Case3

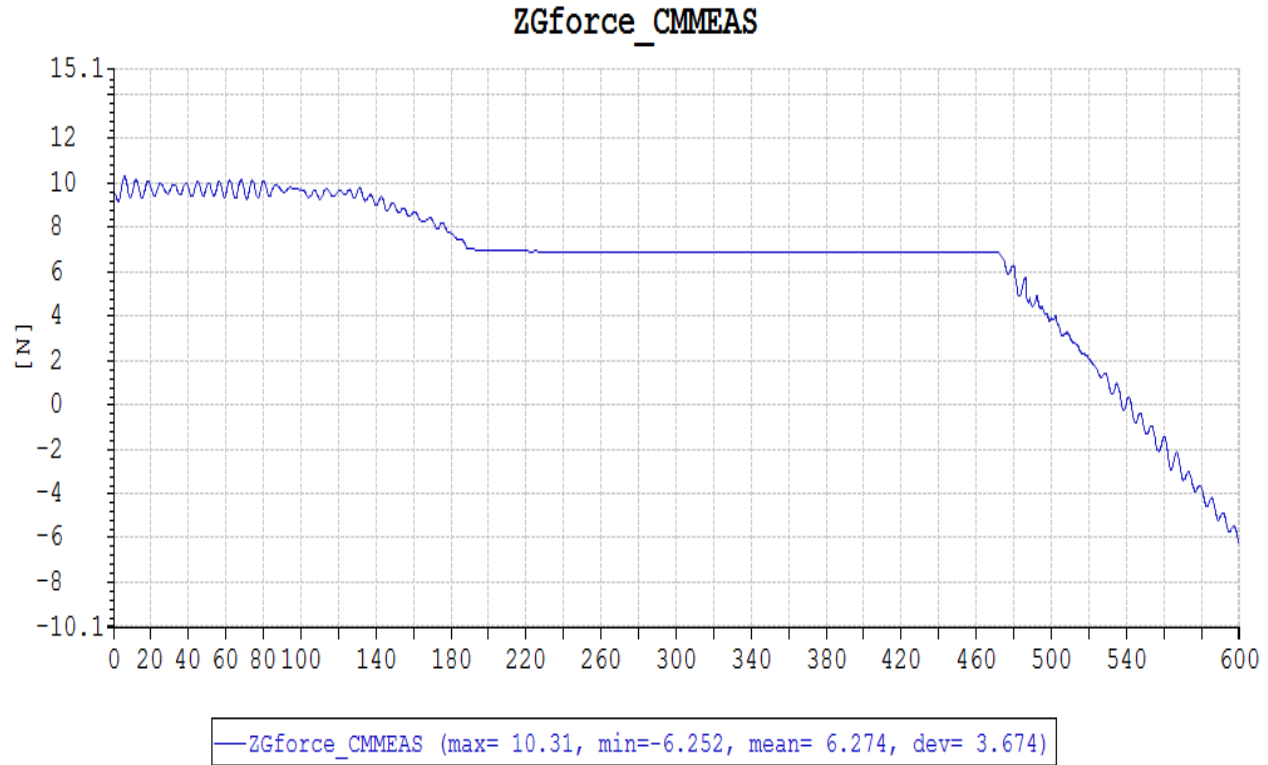


Figure 6.28: Coupling system force in crane wire measurement, Case3

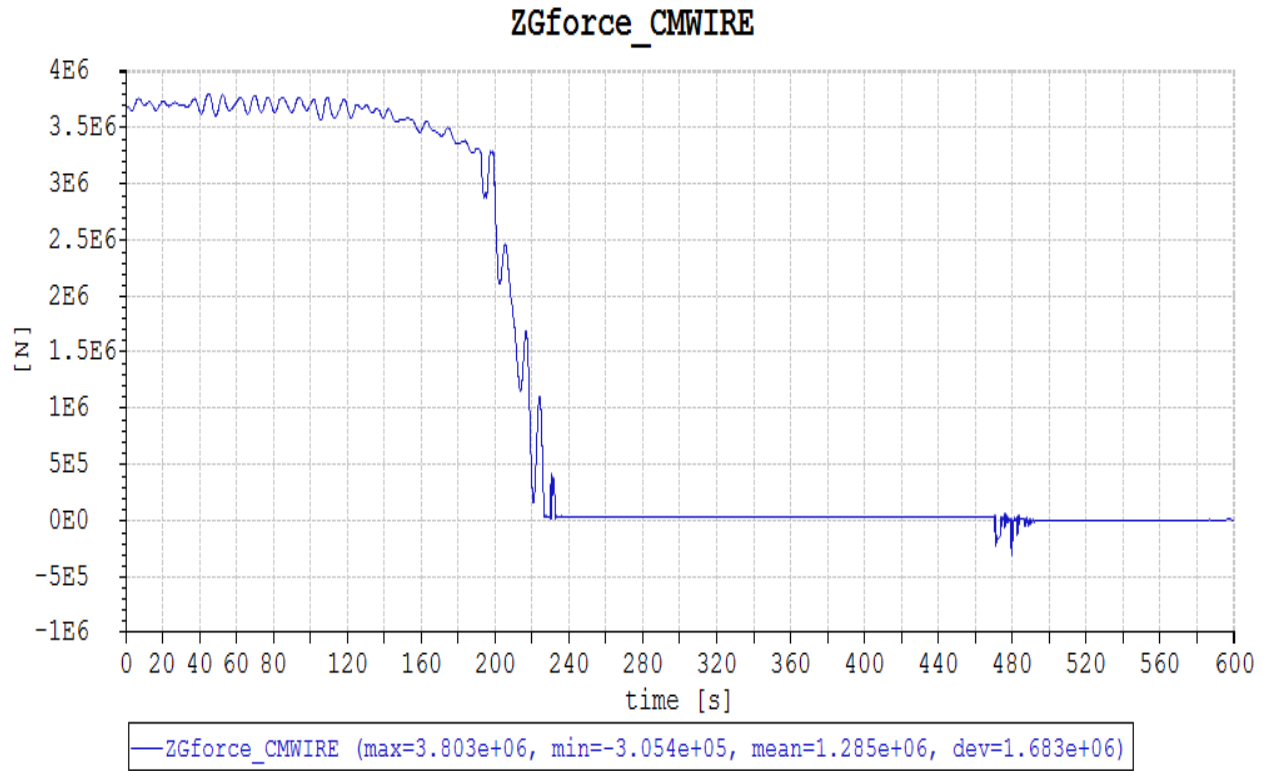


Figure 6.29: Coupling system force in crane wire, Case4

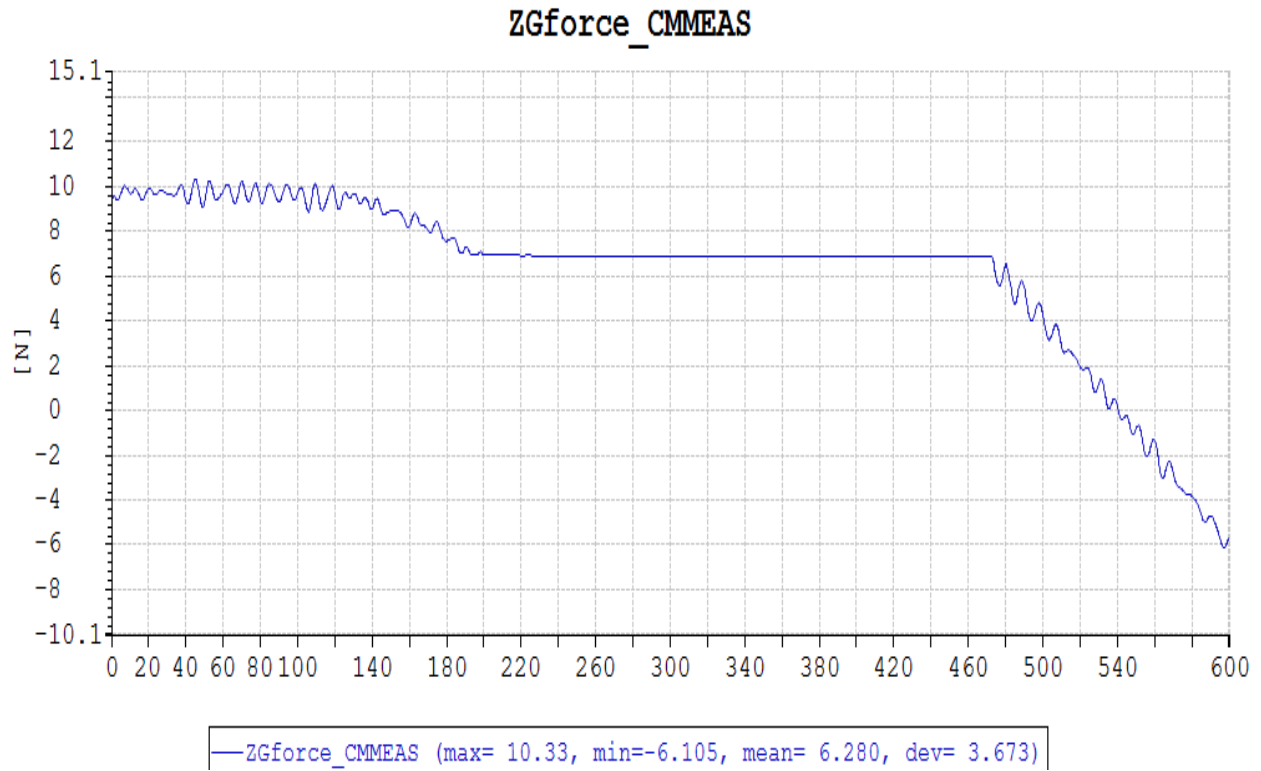


Figure 6.30: Coupling system force in crane wire measurement, Case4

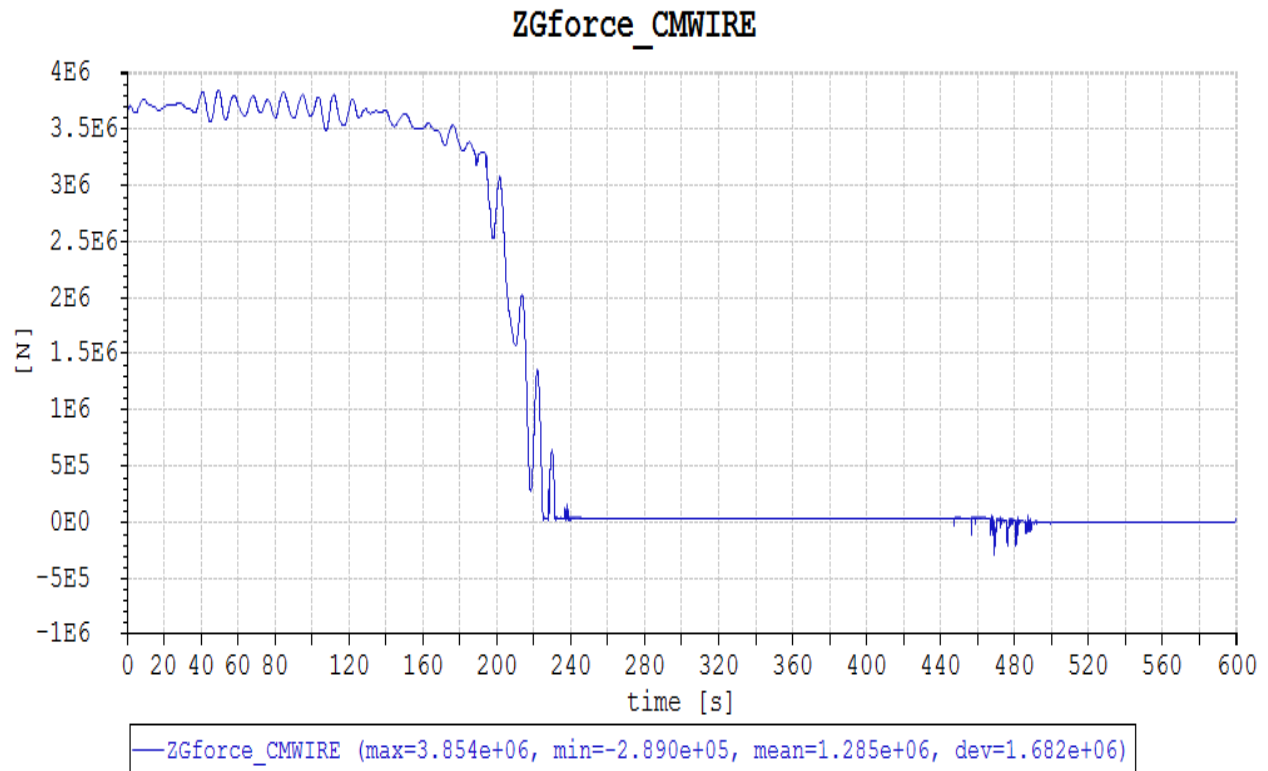


Figure 6.31: Coupling system force in crane wire, Case5

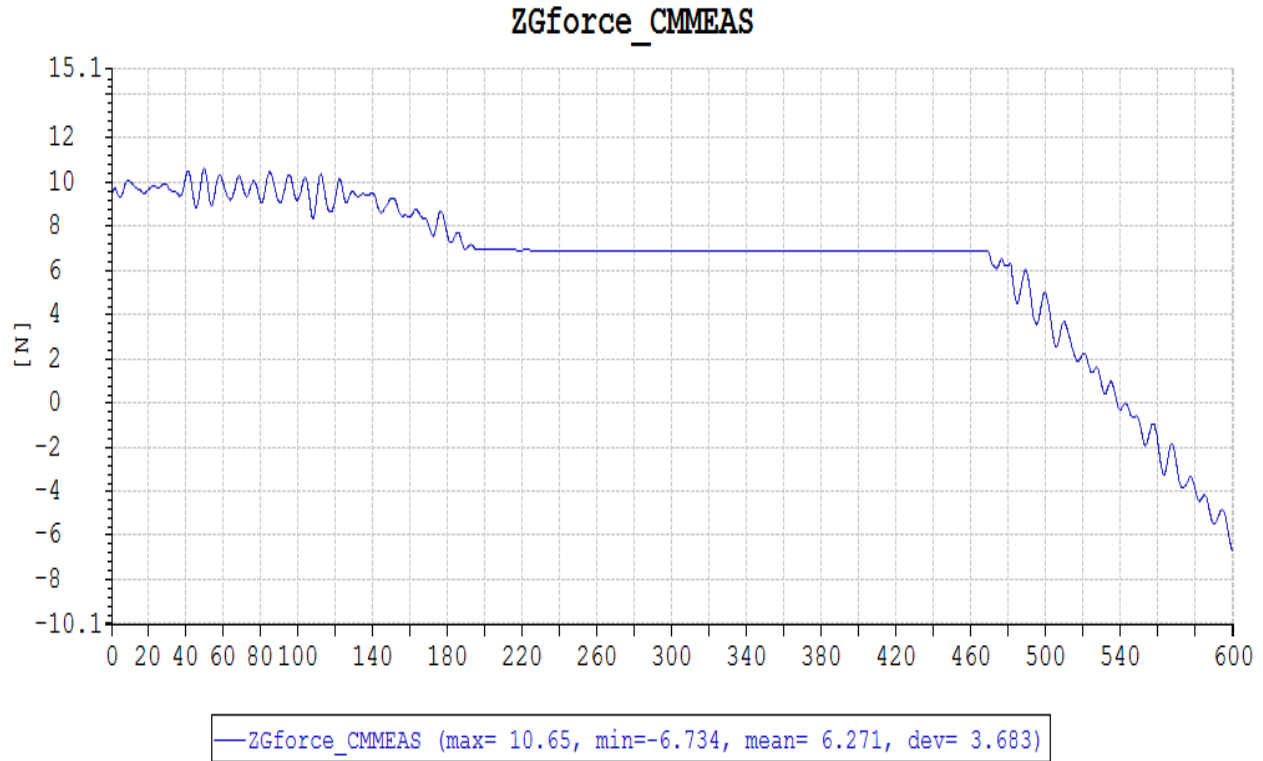


Figure 6.32: Coupling system force in crane wire measurement, Case5

6.2.3 Dynamic analysis of optimized PHC

From the former sections, the optimized stroke is defined as 6.5m to 11m for all the cases, which is 1.5m less than the initial one. So new models with the optimized stroke PHC are established in the same way mentioned in chapter 5 for each case. The only difference is the model of crane wire. A new force elongation interpolation curve will be given with the new stroke but the same slope. Figure 6.33 will illustrate the force characteristic of crane wire with optimized stroke.

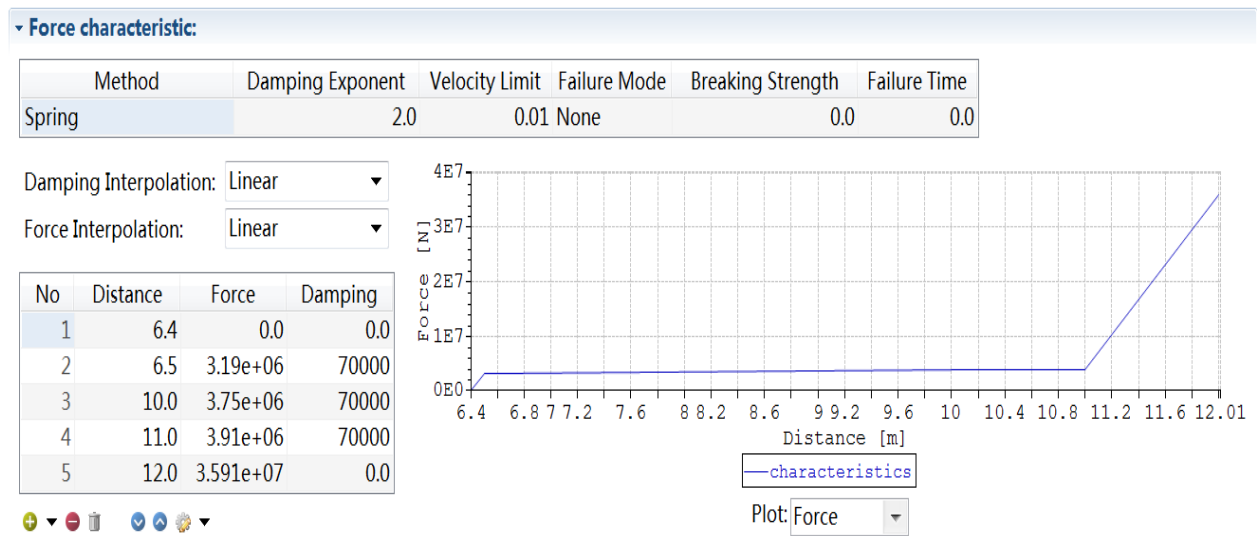


Figure 6.33: Crane wire modelling with optimized stroke in SIMA

After the optimized model established, the static and dynamic analysis are carried out for every case. In order to prove that the optimized PHC has the same influence as the original one with less stroke length, the coupling system force as well as the velocity of the mudmat are compared with the initial stroke models. The results will be presented in the following figures.

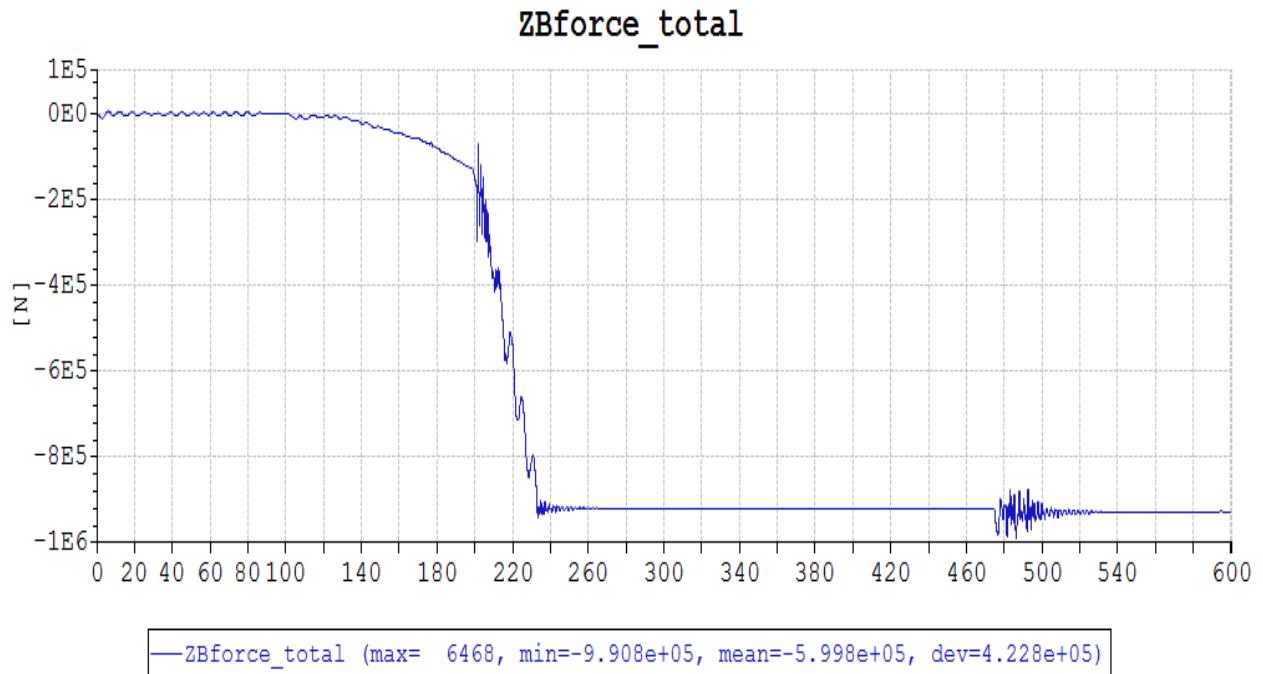


Figure 6.34: Vertical coupling force in Mudmat FS with optimized PHC, Case1

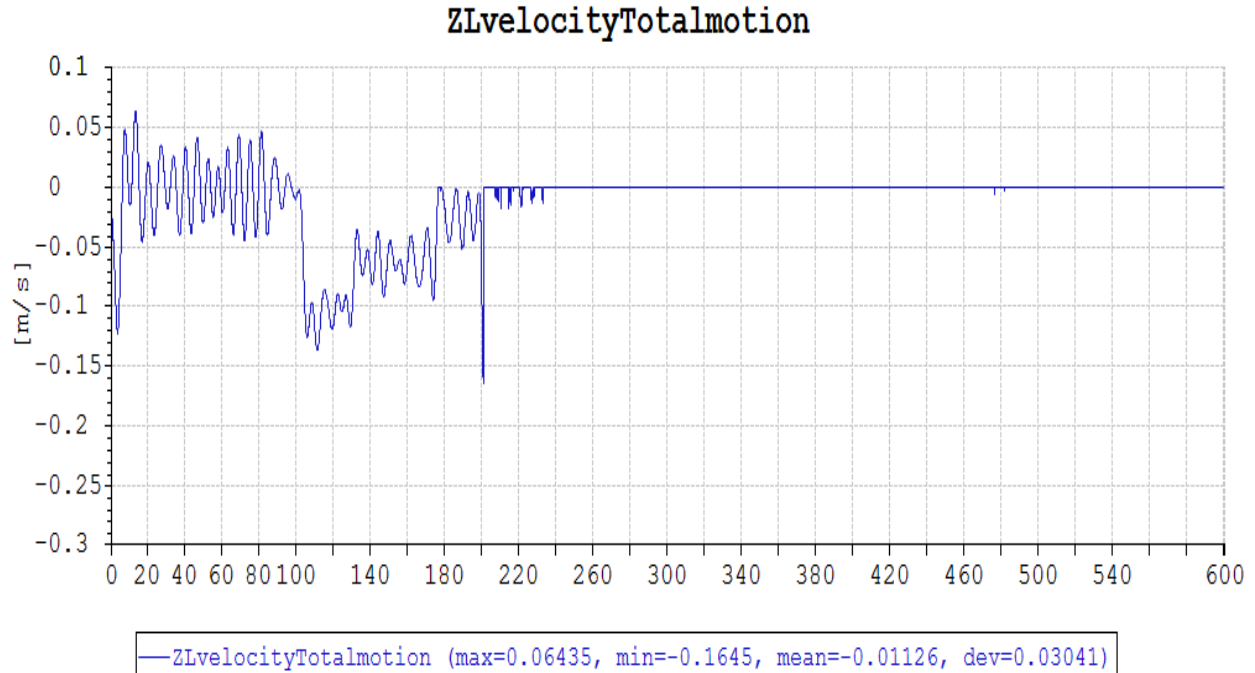


Figure 6.35: Vertical velocity of Mudmat FS with optimized PHC, Case1

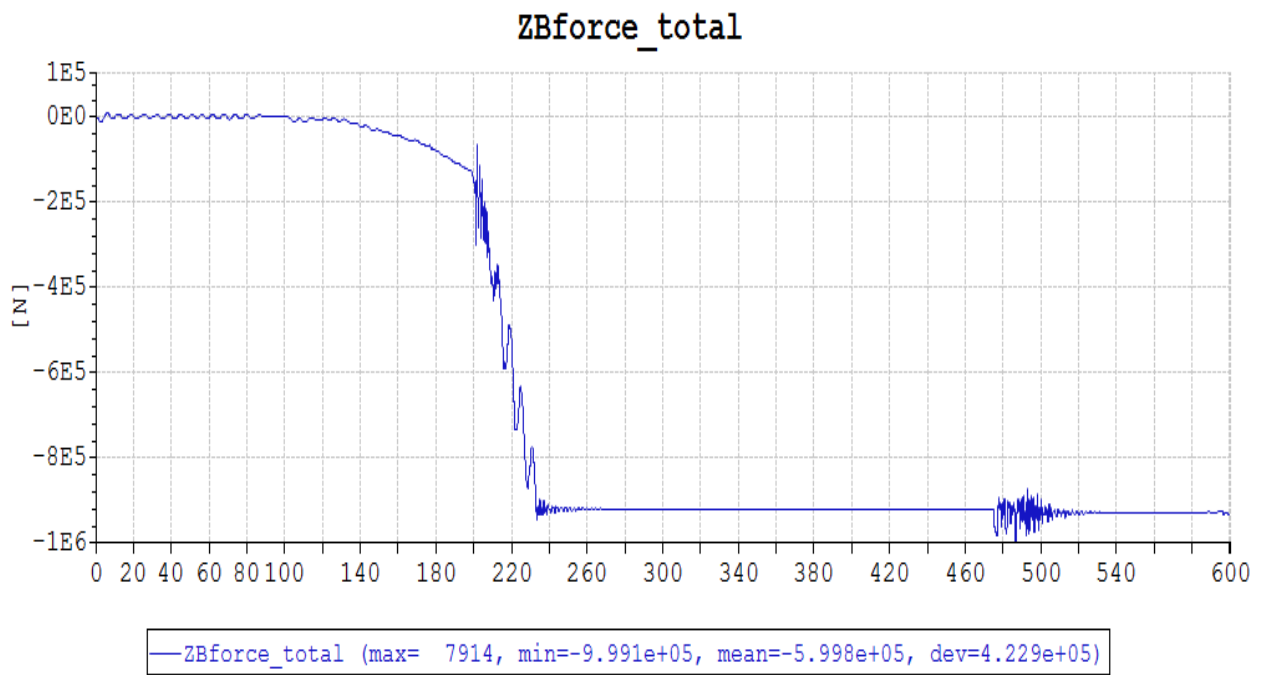


Figure 6.36: Vertical coupling force in Mudmat FS with optimized PHC, Case2

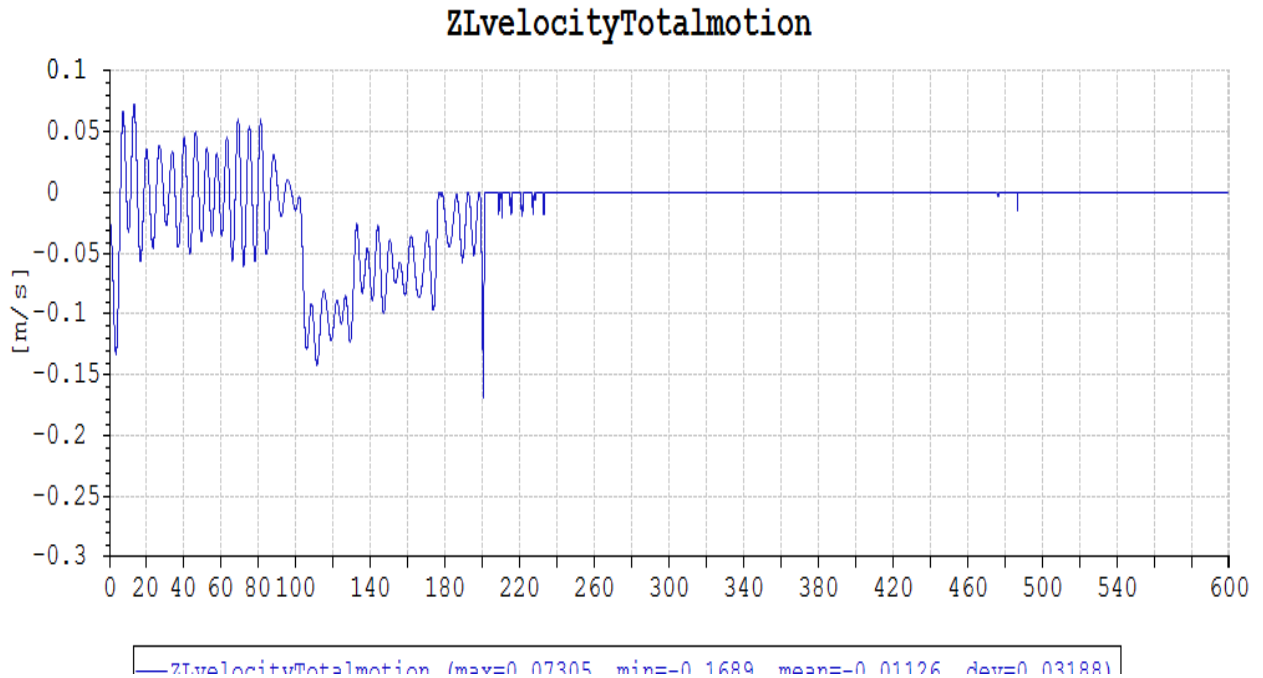


Figure 6.37: Vertical velocity of Mudmat FS with optimized PHC, Case2

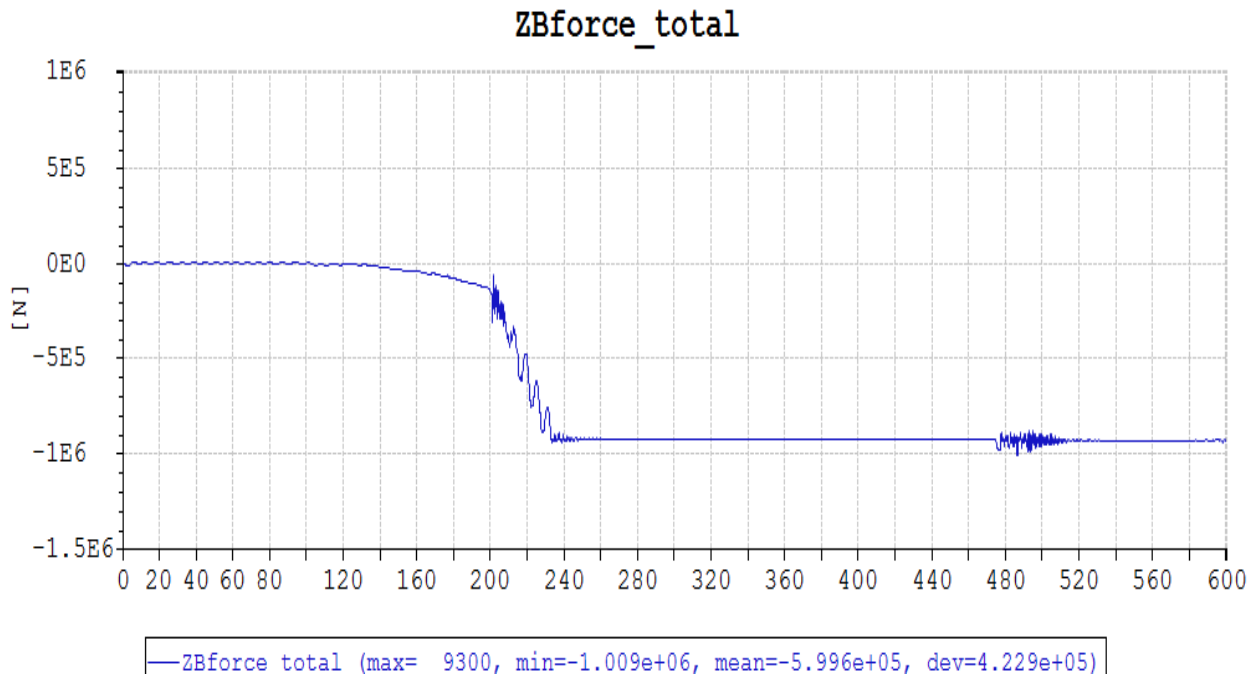


Figure 6.38: Vertical coupling force in Mudmat FS with optimized PHC, Case3

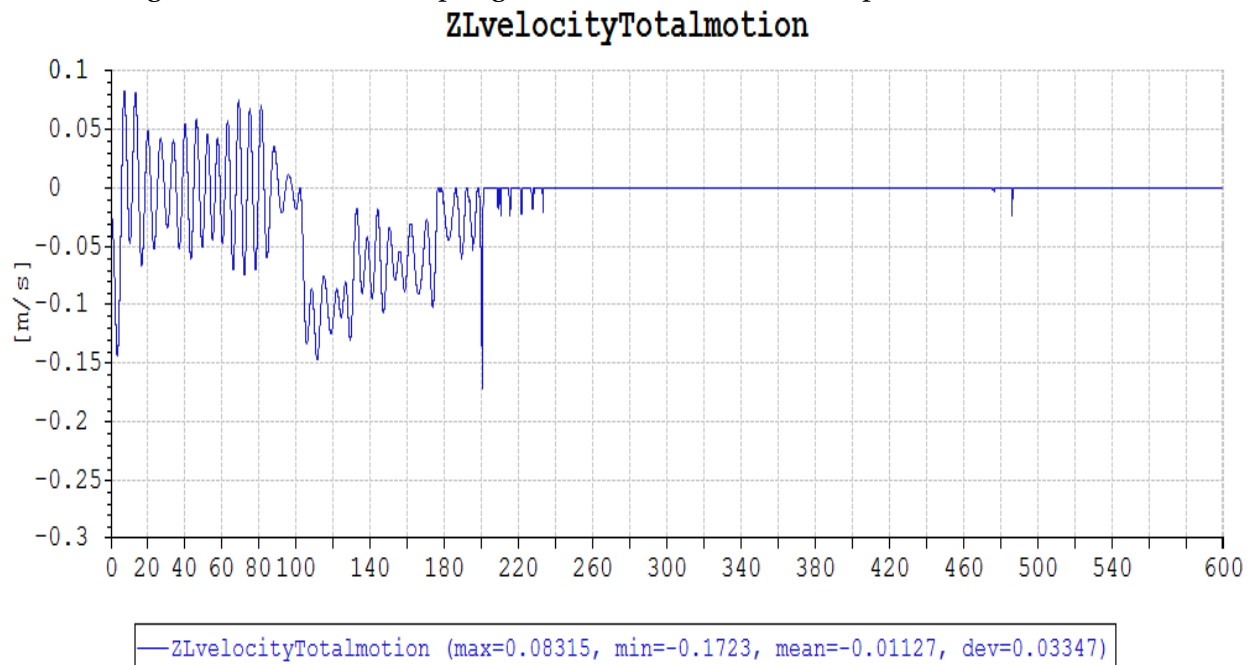


Figure 6.39: Vertical velocity of Mudmat FS with optimized PHC, Case3

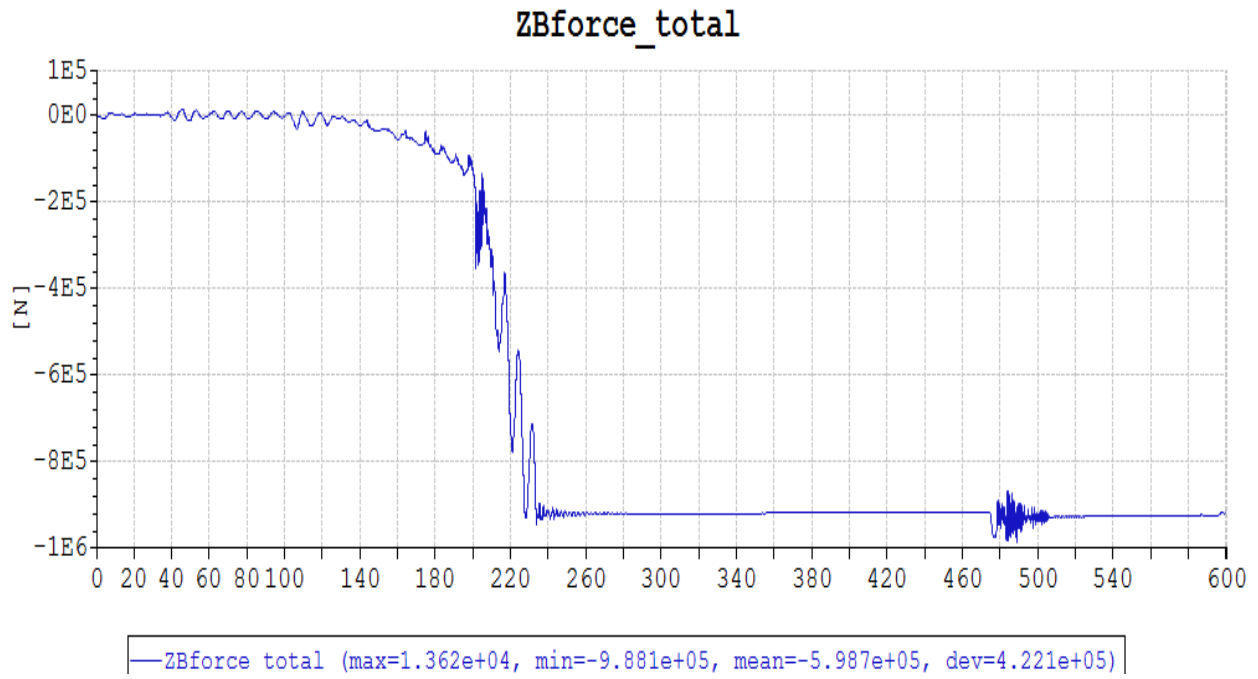


Figure 6.40: Vertical coupling force in Mudmat FS with optimized PHC, Case4

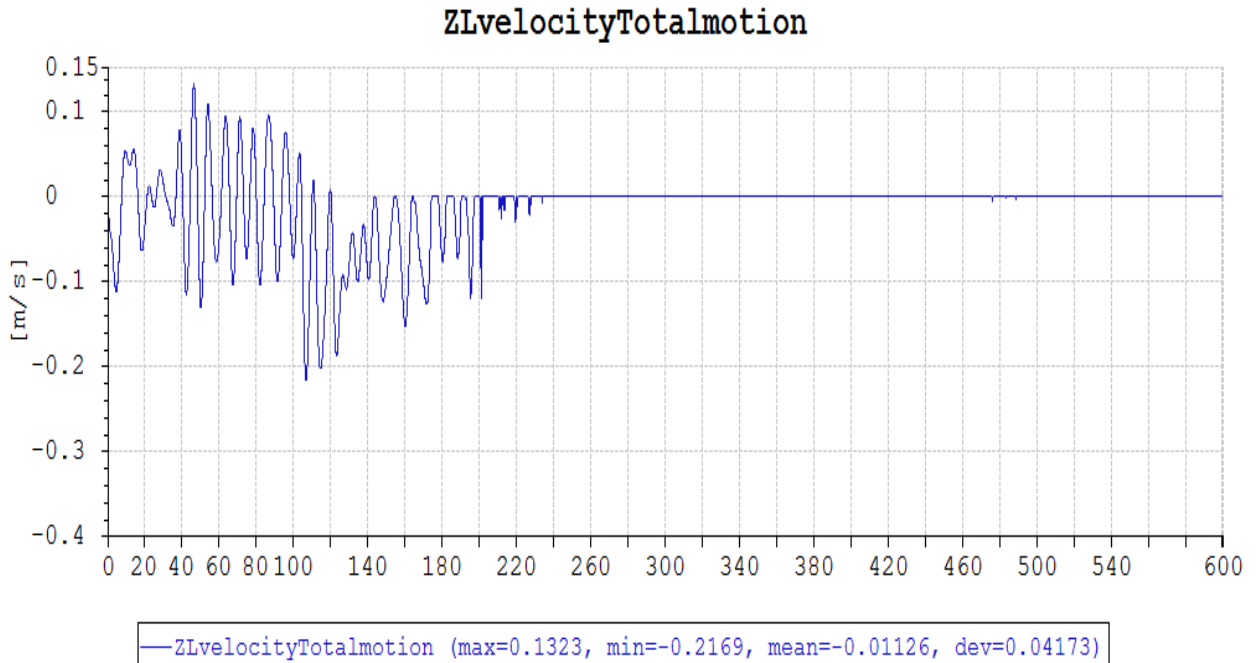


Figure 6.41: Vertical velocity of Mudmat FS with optimized PHC, Case4

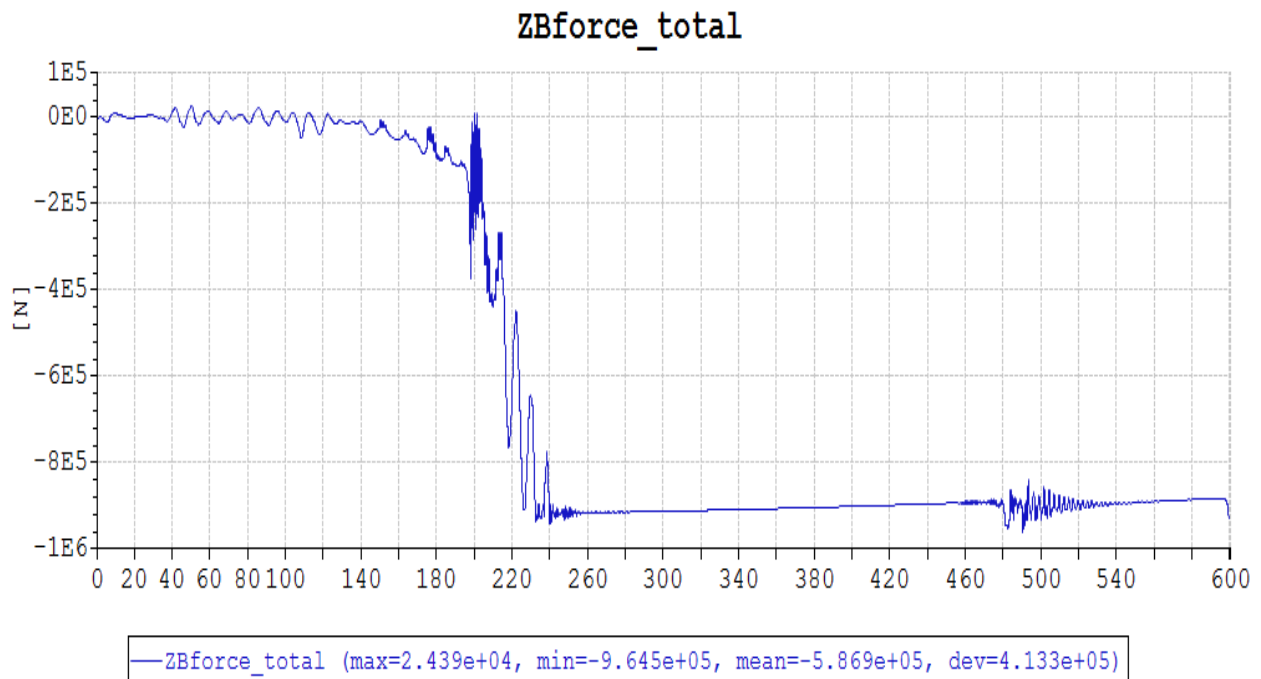


Figure 6.42: Vertical coupling force in Mudmat FS with optimized PHC, Case5

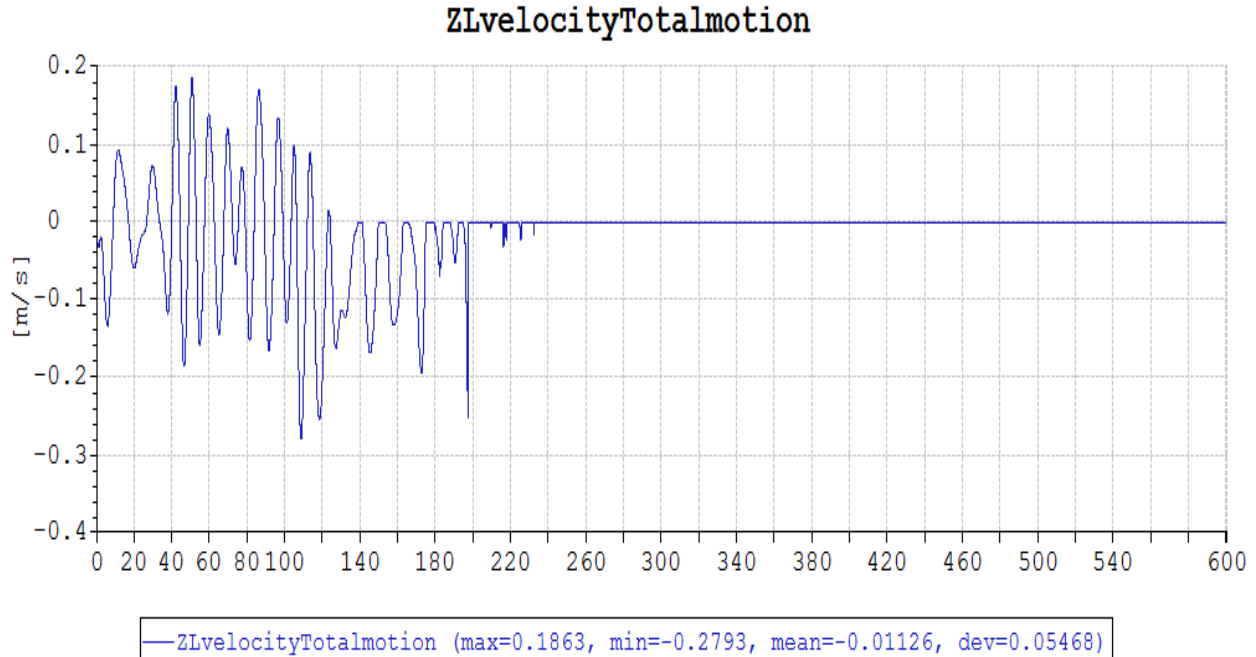


Figure 6.43: Vertical velocity of Mudmat FS with optimized PHC, Case5

6.3 Discussion

The static and dynamic analysis results presented in this chapter illustrate that the influence of PHC and how the optimized stroke is obtained. In this section, all the results will be discussed in order to draw the conclusions at last.

All the demanded results are plotted in this chapter and a post processor process is performed to eliminated the effects of the limits of SIMA program. In order to demonstrate that the passive heave compensator has a positive influence on heavy lift operation, the coupling system force and velocity of the mudmat are compared between the models with and without PHC. The mudmat belongs to the manifold and protection structure in SIMA program and it is the object contacted with the seabed directly. Thus, it might be destroyed by the violent collision with the soil. The application of PHC is aimed to reduce the force and motion of the contacting object and prevent the structure away from the destroy. As a result of that, the positive influence of PHC can be proved when the coupling system force and velocity of the mudmat are alleviated compared with the case without PHC.

Table 6.7 and 6.8 compare the results of vertical coupling system force and velocity with and without PHC respectively.

Table 6.7: Vertical coupling system force in Mudmat FS

Case number		Maximum value[N]	Minimum value[N]	Mean Value[N]	Deviation[N]
1	With PHC	6.47E+03	-9.34E+05	-4.47E+05	4.36E+05
	No PHC	1.27E+05	-9.84E+05	-5.34E+05	4.57E+05
	Ratio	0.05	0.95	0.84	0.96
2	With PHC	8.09E+03	-9.45E+05	-4.47E+05	4.36E+05
	No PHC	1.26E+05	-9.27E+05	-5.13E+05	4.38E+05
	Ratio	0.06	1.02	0.87	1.00
3	With PHC	9.30E+03	-9.48E+05	-4.47E+05	4.36E+05
	No PHC	1.54E+05	-9.28E+05	-5.13E+05	4.39E+05
	Ratio	0.06	1.02	0.87	0.99
4	With PHC	1.55E+04	-9.42E+05	-4.47E+05	4.36E+05
	No PHC	1.54E+05	-9.42E+05	-5.14E+05	4.38E+05
	Ratio	0.10	1.00	0.87	1.00
5	With PHC	2.44E+04	-9.63E+05	-4.43E+05	4.32E+05
	No PHC	1.98E+05	-9.47E+05	-5.00E+05	4.27E+05
	Ratio	0.12	1.02	0.89	1.01

The ratio is equal to the value with PHC divided by that without PHC. It means that the vertical coupling system force is alleviated by PHC when the ratio is less than 1. Therefore, it shows that the maximum and mean value of the vertical coupling system force in Mudmat FS are reduced by PHC while the minimum value and deviation don't change much when PHC is applied by Table 6.7.

Moreover from case 1 to case 3, the peak period $T_p=2m$ for all the three cases while the significant wave height H_s increases from 2m to 3m but the ratio doesn't change a lot. However, the ratio decrease from case 1 to case 4 and case 5, which have the same $H_s=2.5m$ but increasing T_p from 6s to 10s. It implies that the influence of PHC on vertical force is peak period T_p sensitive compared with significant height H_s .

Table 6.8: Vertical global velocity of Mudmat FS

Case number		Max. value[m/s]	Min. value[m/s]	Mean Value[m/s]	Deviation[m/s]
1	With PHC	6.43E-02	-1.77E-01	-1.69E-02	3.66E-02
	No PHC	4.45E-01	-4.50E-01	-1.56E-02	1.42E-01
	Ratio	0.14	0.39	1.08	0.26
2	With PHC	7.23E-02	-1.92E-01	-1.69E-02	3.85E-02
	No PHC	4.44E-01	-4.40E-01	-1.56E-02	1.44E-01
	Ratio	0.16	0.44	1.09	0.27
3	With PHC	8.32E-02	-2.01E-01	-1.69E-02	4.05E-02
	No PHC	4.92E-01	-4.88E-01	-1.56E-02	1.60E-01
	Ratio	0.17	0.41	1.09	0.25
4	With PHC	1.32E-01	-2.90E-01	-1.69E-02	5.12E-02
	No PHC	4.95E-01	-5.77E-01	-1.56E-02	1.62E-01
	Ratio	0.27	0.50	1.09	0.32
5	With PHC	1.86E-01	-2.79E-01	-1.69E-02	6.63E-02
	No PHC	5.61E-01	-5.60E-01	-1.56E-02	1.60E-01
	Ratio	0.33	0.50	1.08	0.41

As for the vertical global velocity of mudmat FS, the ratio is all far away lower than 1 except the ratio of mean value is close to 1. As a result of that, it proves that the passive heave compensator helps to reduce the vertical motion of the mudmat during heavy lift operation. Similarly compared the ratio between case 1, 2, 3 and case 1, 4, 5, it can be concluded that the influence of PHC on vertical motion is peak period T_p sensitive compared with significant height H_s .

In the former sections, it is introduced that how the optimized stroke is obtained and the results

of model with optimized PHC are also plotted. In order to demonstrate that the optimized PHC can provide the same influence with less stroke length. A compare between the initial and optimized PHC is presented in Table 6.9 and 6.10.

The ratio in Table 6.9 and 6.10 is the value with initial PHC divided by that with optimized PHC. It's obvious that all the ratio is close to 1, which implies that the PHC with optimized stroke has the same effect as the initial one with less stroke length.

Table 6.9: Vertical coupling system force in Mudmat FS compared between optimized and initial PHC

Case number		Max. value[N]	Min. value[N]	Mean Value[N]	Deviation[N]
1	Initial PHC	6.47E+03	-9.34E+05	-4.47E+05	4.36E+05
	Optimized PHC	6.47E+03	-9.40E+05	-4.37E+05	4.34E+05
	Ratio	1.00	0.99	1.02	1.00
2	Initial PHC	8.09E+03	-9.45E+05	-4.47E+05	4.36E+05
	Optimized PHC	7.91E+03	-9.46E+05	-4.37E+05	4.34E+05
	Ratio	1.02	1.00	1.02	1.00
3	Initial PHC	9.30E+03	-9.48E+05	-4.47E+05	4.36E+05
	Optimized PHC	9.30E+03	-9.44E+05	-4.37E+05	4.35E+05
	Ratio	1.00	1.00	1.02	1.00
4	Initial PHC	1.55E+04	-9.42E+05	-4.47E+05	4.36E+05
	Optimized PHC	1.36E+04	-9.44E+05	-4.37E+05	4.34E+05
	Ratio	1.14	1.00	1.02	1.00
5	Initial PHC	2.44E+04	-9.63E+05	-4.43E+05	4.32E+05
	Optimized PHC	2.44E+04	-9.43E+05	-4.33E+05	4.30E+05
	Ratio	1.00	1.02	1.02	1.00

Table 6.10: Vertical global velocity of Mudmat FS compared between optimized and initial PHC

Case number		Max. value[m/s]	Min. value[m/s]	Mean Value[m/s]	Deviation[m/s]
1	Initial PHC	6.43E-02	-1.77E-01	-1.69E-02	3.66E-02
	Optimized PHC	6.43E-02	-1.65E-01	-1.69E-02	3.60E-02
	Ratio	1.00	1.07	1.00	1.02
2	Initial PHC	7.23E-02	-1.92E-01	-1.69E-02	3.85E-02
	Optimized PHC	7.30E-02	-1.69E-01	-1.69E-02	3.78E-02
	Ratio	0.99	1.14	1.00	1.02
3	Initial PHC	8.32E-02	-2.01E-01	-1.69E-02	4.05E-02
	Optimized PHC	8.32E-02	-1.72E-01	-1.69E-02	3.98E-02
	Ratio	1.00	1.16	1.00	1.02
4	Initial PHC	1.32E-01	-2.90E-01	-1.69E-02	5.12E-02
	Optimized PHC	1.32E-01	-2.17E-01	-1.69E-02	5.02E-021
	Ratio	1.00	1.34	1.00	1.02
5	Initial PHC	1.86E-01	-2.79E-01	-1.69E-02	6.63E-02
	Optimized PHC	1.86E-01	-2.79E-011	-1.69E-02	6.63E-02
	Ratio	1.00	1.00	1.00	1.00

Chapter 7

Conclusion

7.1 Conclusion

The objective of this thesis is to demonstrate that the passive heave compensator can reduce the vertical forces and motions during heavy lift operation and determine the optimum heave compensator stroke setting. All the conclusions are drawn from the results and discussion in Chapter 6.

It shows that the maximum and mean value of the vertical coupling system force in Mudmat FS are reduced by PHC while the minimum value and deviation don't change much when PHC is applied by Table 6.7. Meanwhile, the ratio is all far away lower than 1.0 except the ratio of mean value is close to 1 in Table 6.8.

As a result of that, it proves that the passive heave compensator can be applied to alleviate the vertical forces as well as motions during heavy lift operation. Moreover, it can be concluded that the influence of passive heave compensator is peak period sensitive by comparing the results in different environment condition cases.

As for the optimization of the passive heave compensator, the optimum stroke can be calculated from the force varied range in the crane wire. And the PHC with optimized stroke has the same effect as the initial one with less stroke length.

7.2 Recommendations for further work

The thesis provides a comprehensive understanding of the influence of passive heave compensator during heavy lift operation by simulating the process of penetrating into seabed in SIMA program. However, there still exists some other tasks which can be fulfilled in the further work. These recommendations for further work are listed below:

- More complex environment conditions. Due to the limit of time, only five environment conditions are carried out in this thesis. In the further study, more sea states with the characteristics of wave, wind and current can be taken into consideration to study the effects of environment in more detail.
- More process of heavy lift operation. In further study, the other process of heavy lift operation like lowering in the air, lifting through wave zone, deepwater lowering can be added to get more detailed results.
- More force elongation interpolation relationship. In this thesis, only one type of passive heave compensator is applied. It is recommended that the force elongation interpolation relationship can be varied when modelling the PHC to seek more possibilities of the optimized PHC.

Appendix A

Vertical coupling system force in mudmats

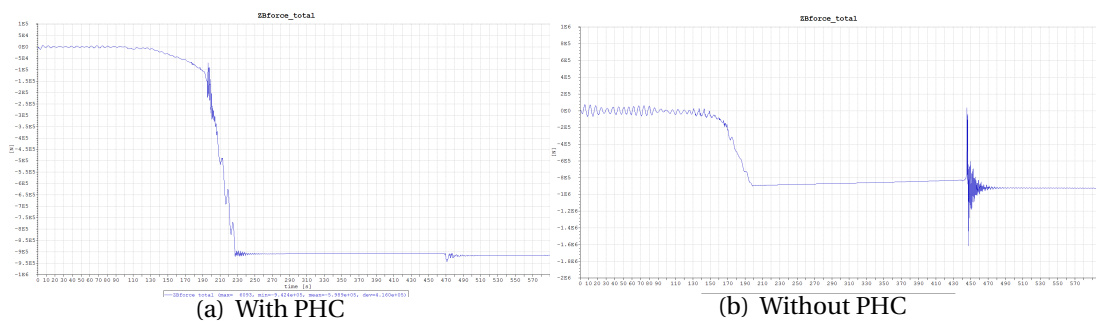


Figure A.1: Vertical coupling system force in Mudmat FP, Case 1

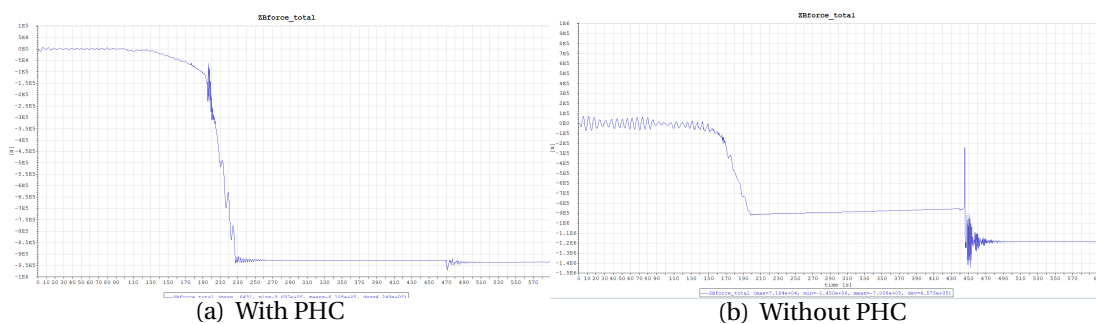


Figure A.2: Vertical coupling system force in Mudmat AS, Case 1

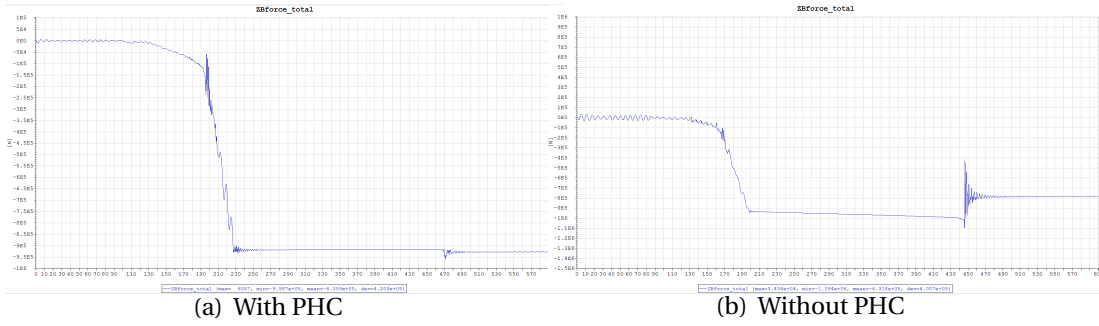


Figure A.3: Vertical coupling system force in Mudmat AP, Case 1

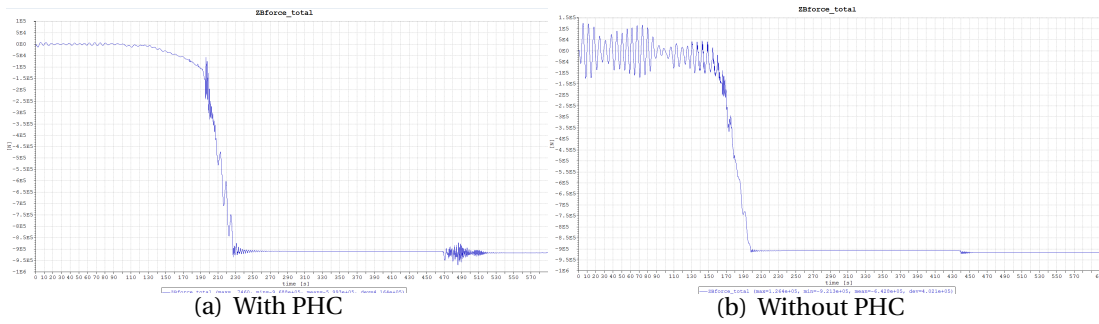


Figure A.4: Vertical coupling system force in Mudmat FP, Case 2

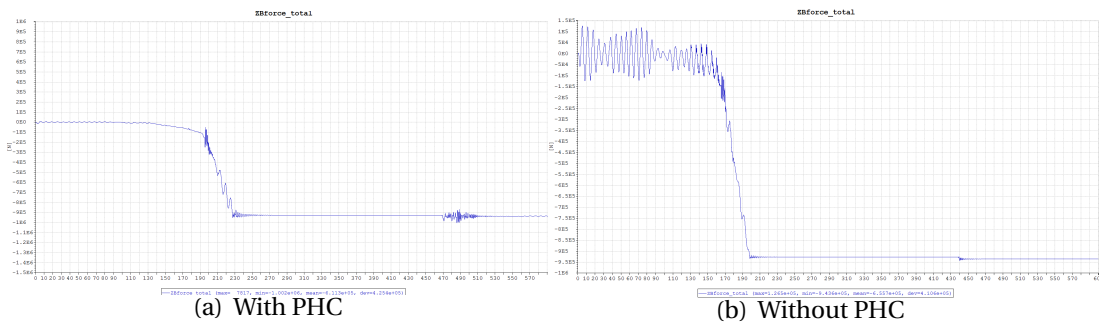


Figure A.5: Vertical coupling system force in Mudmat AS, Case 2

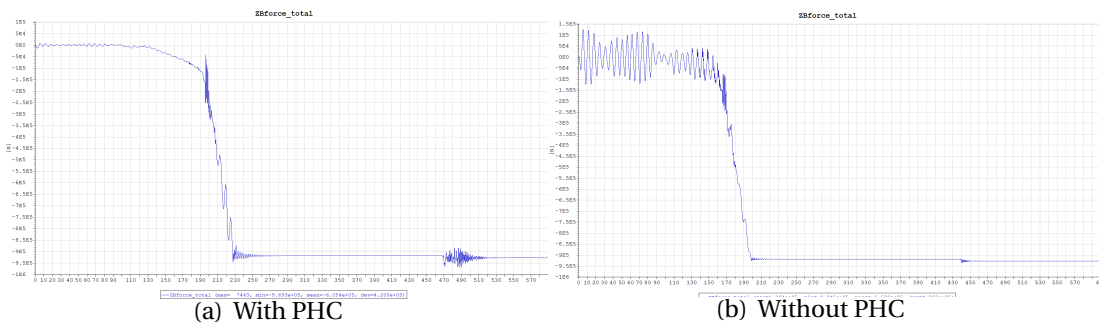


Figure A.6: Vertical coupling system force in Mudmat AP, Case 2

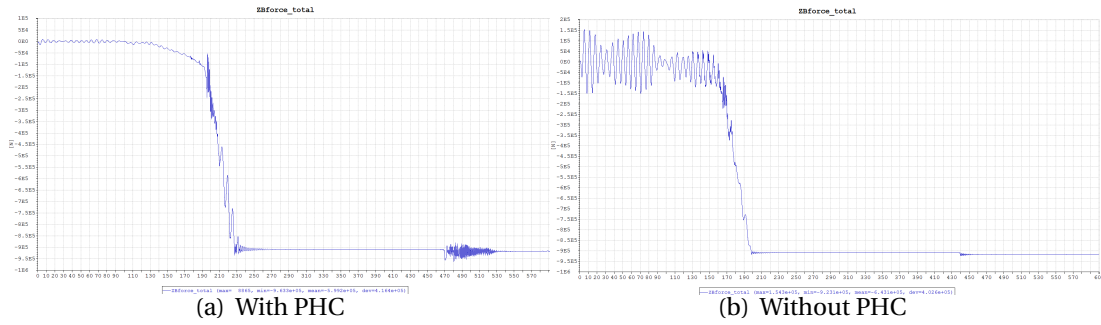


Figure A.7: Vertical coupling system force in Mudmat FP, Case 3

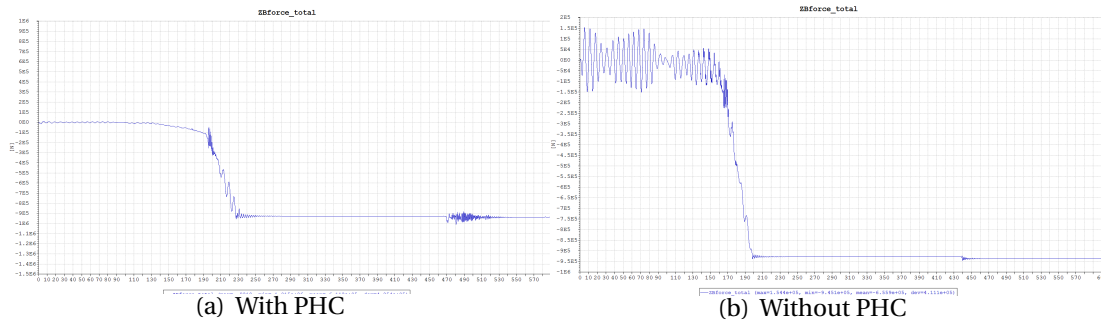


Figure A.8: Vertical coupling system force in Mudmat AS, Case 3

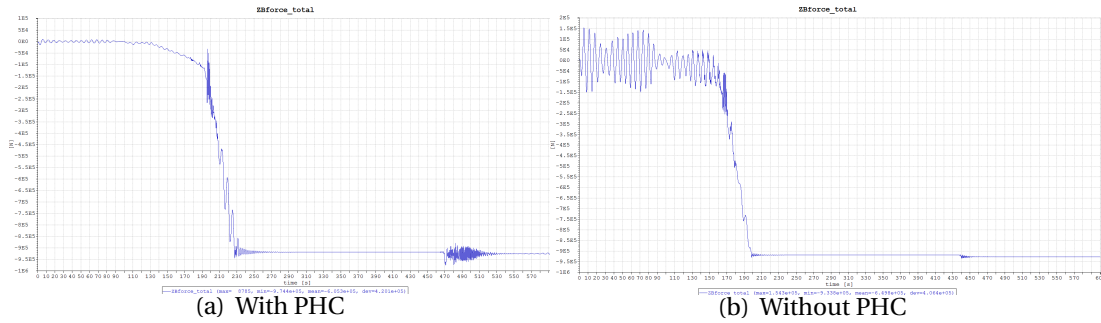


Figure A.9: Vertical coupling system force in Mudmat AP, Case 3

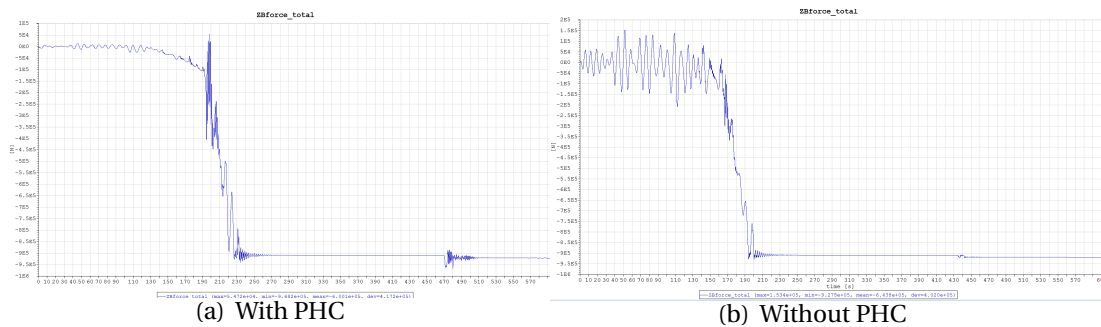


Figure A.10: Vertical coupling system force in Mudmat FP, Case 4

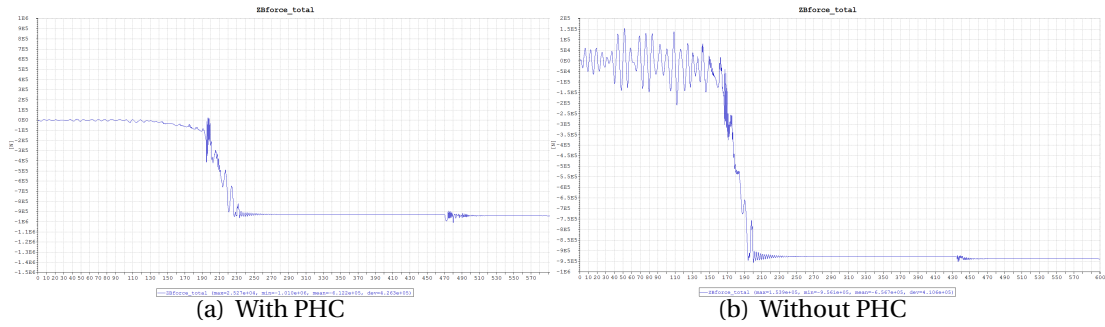


Figure A.11: Vertical coupling system force in Mudmat AS, Case 4

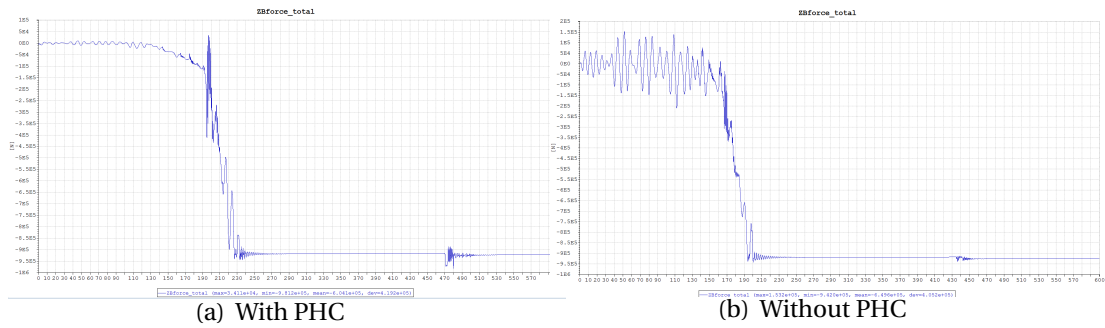


Figure A.12: Vertical coupling system force in Mudmat AP, Case 4

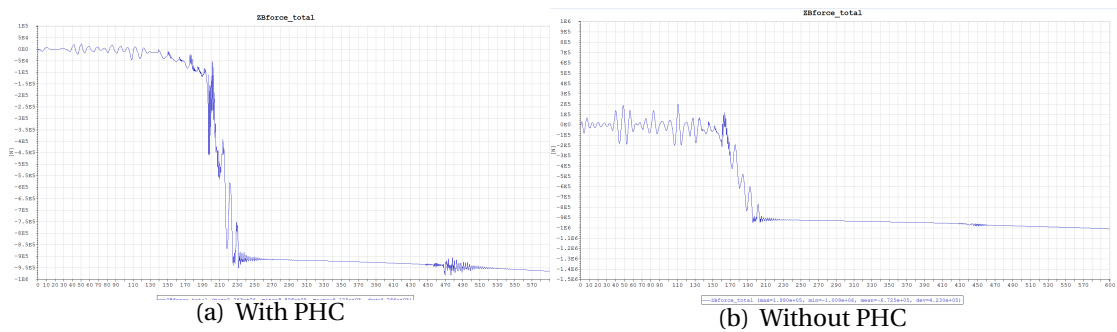


Figure A.13: Vertical coupling system force in Mudmat FP, Case 5

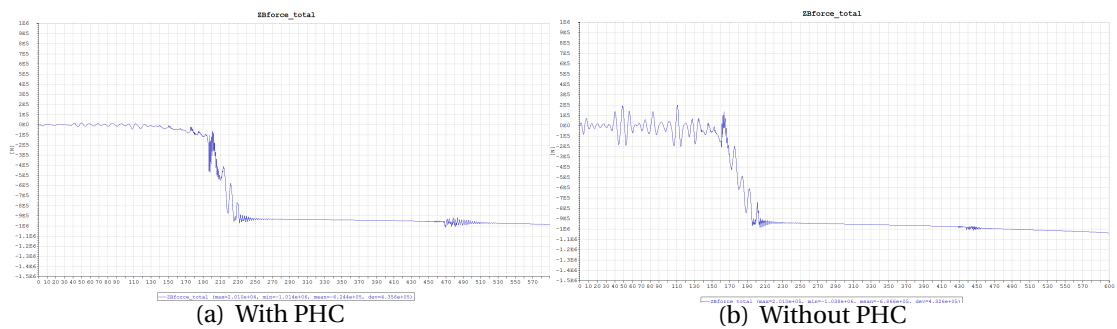


Figure A.14: Vertical coupling system force in Mudmat AS, Case 5

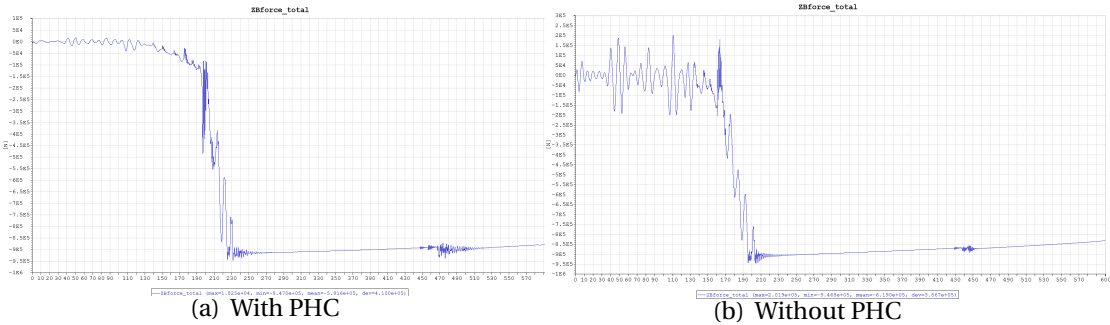


Figure A.15: Vertical coupling system force in Mudmat AP, Case 5

Appendix B

Vertical global velocity of mudmats

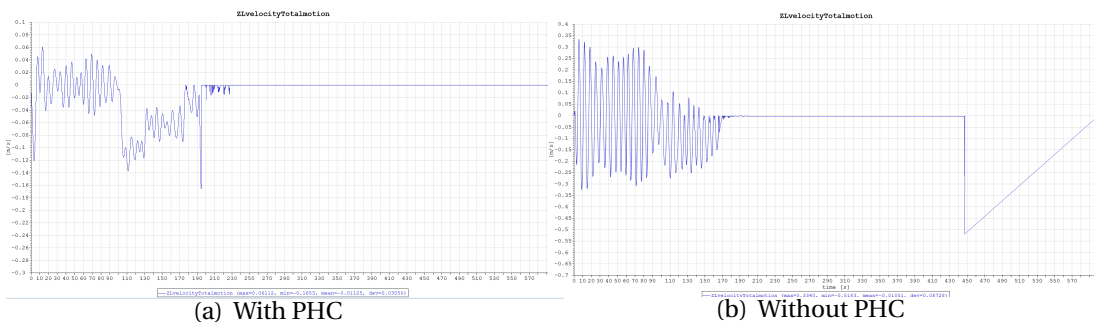


Figure B.1: Vertical global velocity of Mudmat FP, Case 1

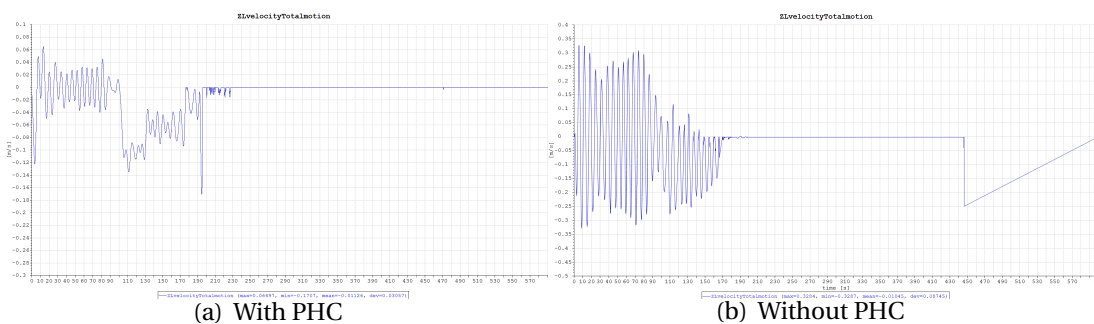


Figure B.2: Vertical global velocity of Mudmat AS, Case 1

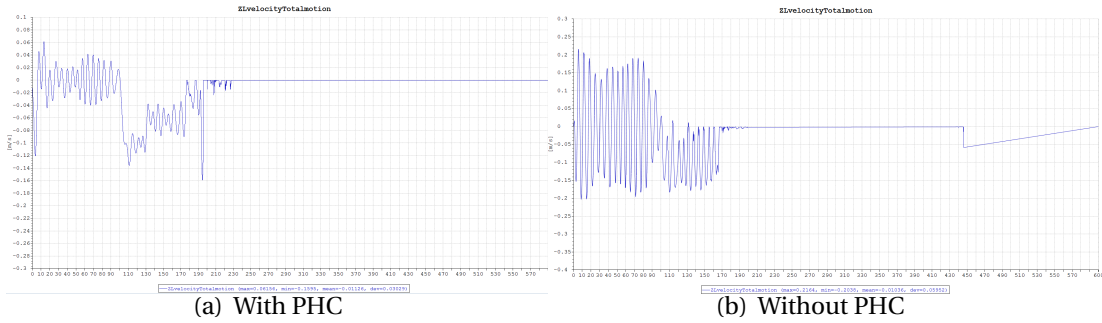


Figure B.3: Vertical global velocity of Mudmat AP, Case 1

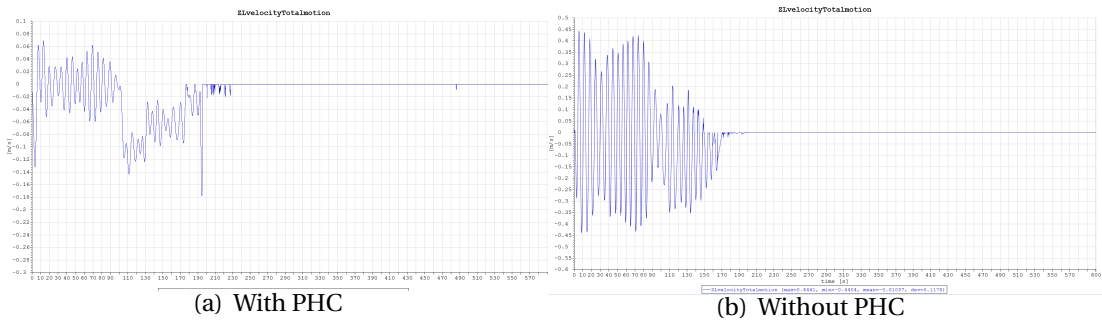


Figure B.4: Vertical global velocity of Mudmat FP, Case 2

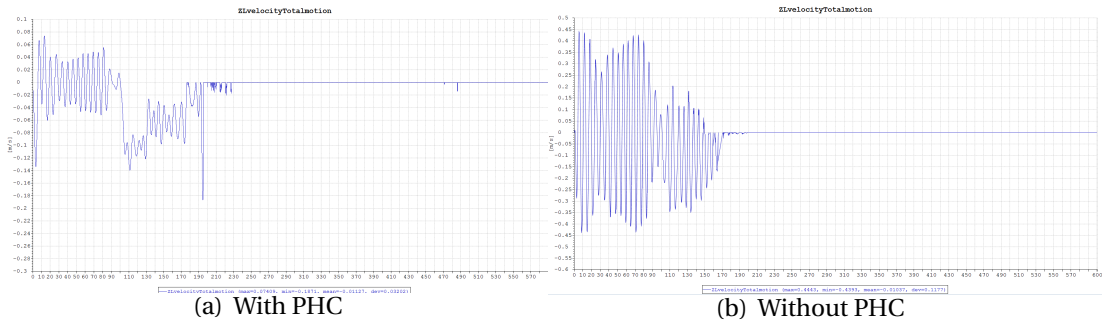


Figure B.5: Vertical global velocity of Mudmat AS, Case 2

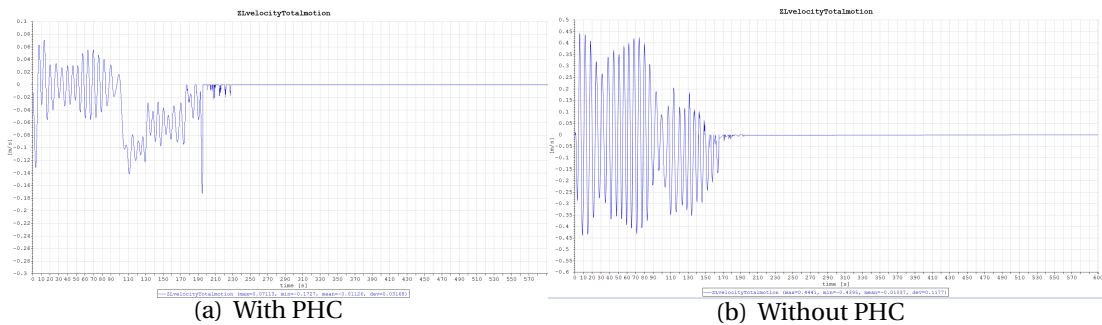


Figure B.6: Vertical global velocity of Mudmat AP, Case 2

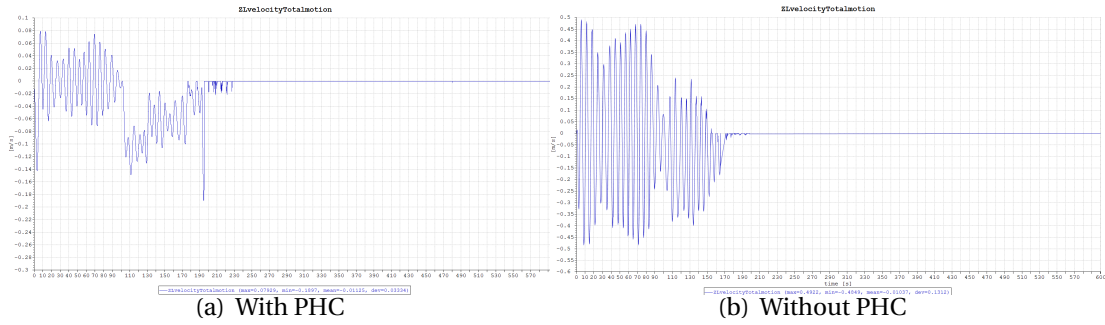


Figure B.7: Vertical global velocity of Mudmat FP, Case 3

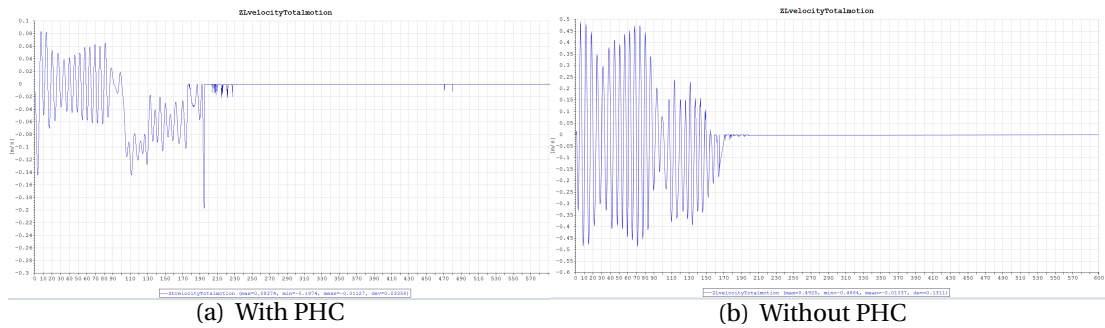


Figure B.8: Vertical global velocity of Mudmat AS, Case 3

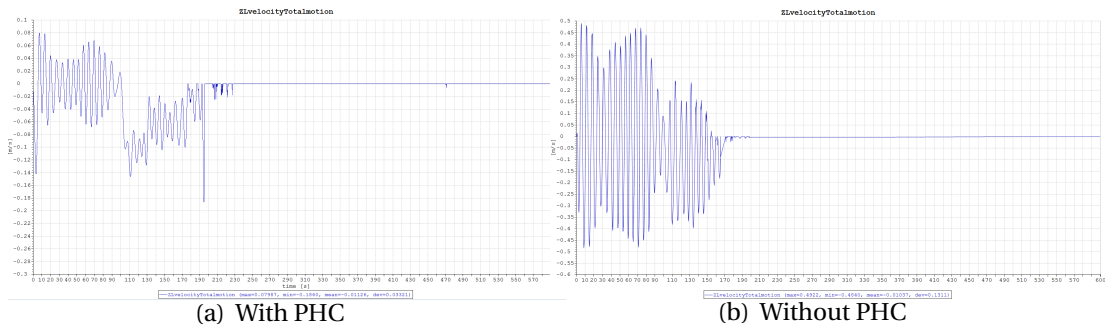


Figure B.9: Vertical global velocity of Mudmat AP, Case 3

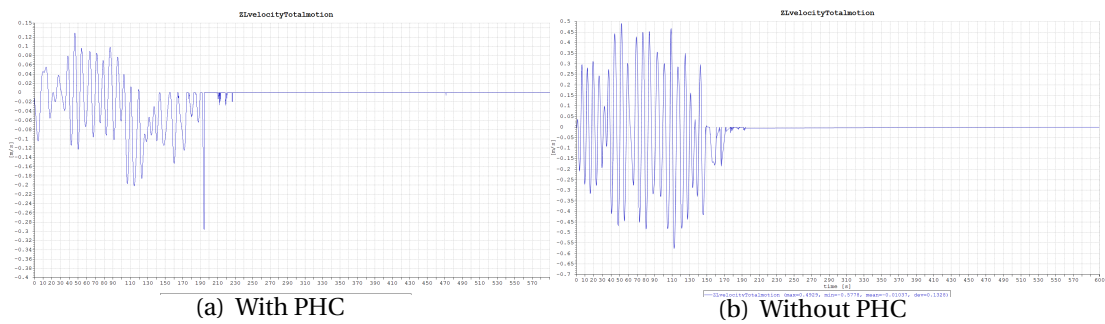


Figure B.10: Vertical global velocity of Mudmat FP, Case 4

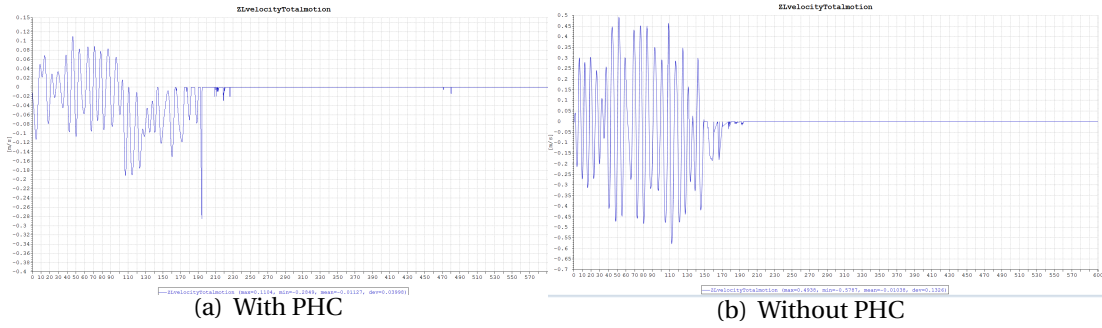


Figure B.11: Vertical global velocity of Mudmat AS, Case 4

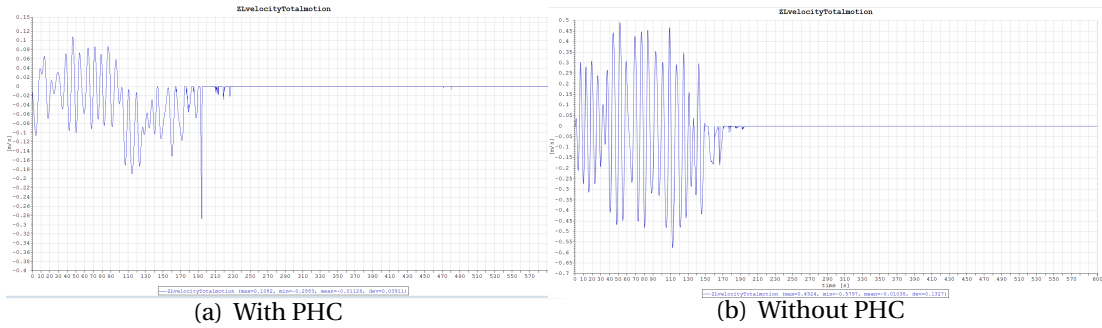


Figure B.12: Vertical global velocity of Mudmat AP, Case 4

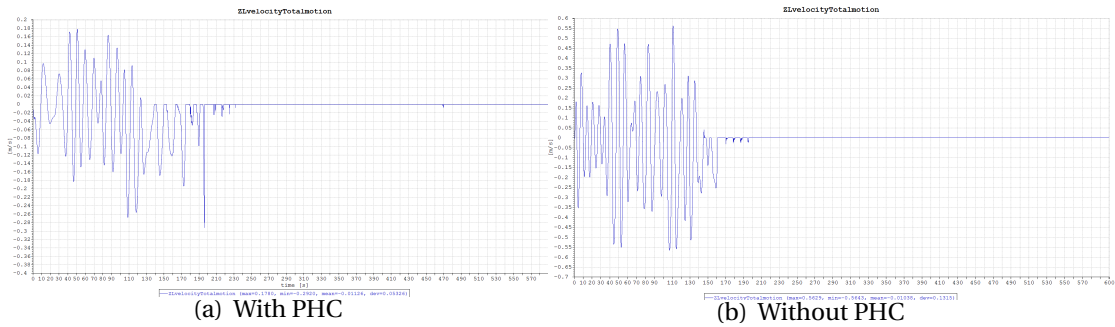


Figure B.13: Vertical global velocity of Mudmat FP, Case 5

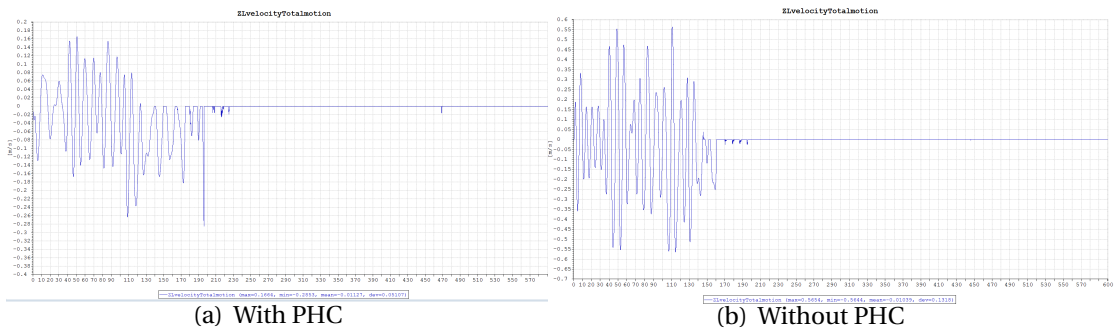


Figure B.14: Vertical global velocity of Mudmat AS, Case 5

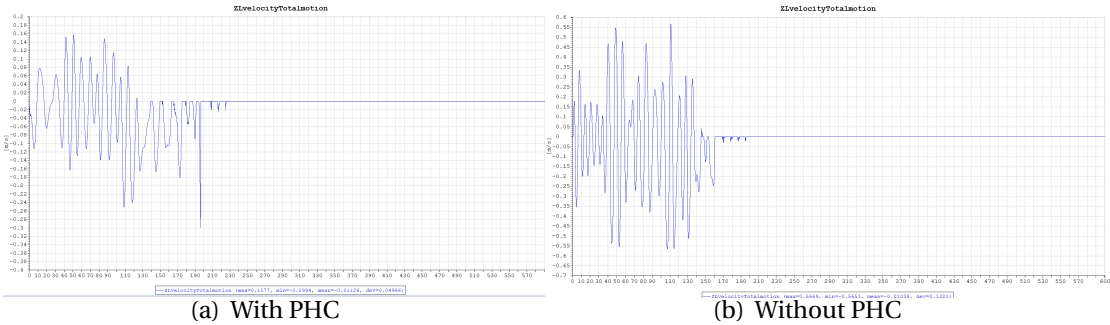


Figure B.15: Vertical global velocity force of Mudmat AP, Case 5

Bibliography

- [1] J. Woodacre, R. Bauer, and R. Irani, “A review of vertical motion heave compensation systems,” *Ocean Engineering*, vol. 104, pp. 140–154, 2015.
- [2] T. Martinsen and A. Totland, *The Engineers Guide*. Norway: Safelink As, 2nd ed., 2012.
- [3] D. Gaddy, “Ultradeep drillship will react to heave with electric-compensating drawworks,” *Oil and Gas Journal*, vol. 95, no. 29, 1997.
- [4] D. N. Veritas, “Dnv-rp-h103 modelling and analysis of marine operations,” *Det Norske Veritas*, 2011.
- [5] *SIMO User Manual*, 2015.
- [6] S. M. E. Jakobsen, “Passive Heave Compensation of Heavy Modules,” 2008.
- [7] B. W. Nam, S. Y. Hong, Y. S. Kim, J. W. Kim, *et al.*, “Effects of passive and active heave compensators on deepwater lifting operation,” *International Journal of Offshore and Polar Engineering*, vol. 23, no. 01, 2013.
- [8] F. R. Driscoll, M. Nahon, and R. G. Lueck, “A comparison of ship-mounted and cage-mounted passive heave compensation systems,” *Journal of Offshore Mechanics and Arctic Engineering*, vol. 122, no. 3, pp. 214–221, 2000.
- [9] A. Keprate, “Impact of passive heave compensator on offshore lifting,” *Journal of Shipping and Ocean Engineering*, vol. 5, no. 4, pp. 166–80, 2015.
- [10] J. T. Hatleskog and M. W. Dunnigan, “Passive compensator load variation for deep-water drilling,” *IEEE Journal of Oceanic Engineering*, vol. 32, no. 3, pp. 593–602, 2007.

- [11] L. R. Robichaux and J. T. Hatleskog, "Semi-active heave compensation system for marine vessels," May 11 1993. US Patent 5,209,302.